Estuarine Shoreline Mapping using Object-based Ensemble Analysis, Aerial Imagery, and LiDAR: A Case Study in the Neuse River Estuary, NC

By

Jessica Richter

May 2022

Director of Thesis: Dr. Hannah Sirianni

Major Department: Geography, Planning, and Environment

Estuarine shorelines are highly dynamic due to their unique geological history, wave and weather conditions, and human modifications to the shoreline. These interactions are heightened as sea level rise intensifies and extreme storms become more frequent due to climate change. Estuarine shoreline classification maps are critical to understanding the context and magnitude of storm-induced erosion as well as ad hoc efforts to shoreline stabilization. Here, an object-based ensemble analysis is used to map natural and engineered shoreline types observed within the Neuse River Estuary (NRE), NC. Object-based ensemble analysis has emerged as a successful framework to improve image classification but has yet to be tested in classifying an estuarine shoreline environment. This approach used *in*-situ reference data, high-resolution aerial imagery, and LiDAR point data to train an ensemble of five machine learning algorithms (Random Forest, Support Vector Machine, LibLINEAR, Artificial Neural Network, and k-Nearest Neighbors). The object-based ensemble produced the highest overall classification accuracy at 76.4% (Kappa value = 0.66), 6.3% higher than the top performing pixel-based model, justifying its use to produce the final shoreline classification map. NRE shoreline change and erosion vulnerability were classified using the object-based image analysis and produced comparable erosion rates to those observed in past studies. The object-based ensemble approach was an effective way to map

shoreline classifications in the NRE and should continue to be explored within other shoreline management applications.

Estuarine Shoreline Mapping using Object-based Ensemble Analysis, Aerial Imagery, and LiDAR: A Case Study in the Neuse River Estuary, NC

A Thesis

Presented to the Faculty of the Department of Geography, Planning, and Environment

East Carolina University

In Partial Fulfillment of the Requirements for the Degree

Master of Science in Geography

by

Jessica Richter

May 2022

Estuarine Shoreline Mapping using Object-based Ensemble Analysis, Aerial imagery, and LiDAR: A Case Study in the Neuse River Estuary, NC

By

Jessica Richter

APPROVED BY:

Director of Thesis _____
(Hannah Sirianni, PhD)

Committee Member _____
(Thad Wasklewicz, PhD)

Committee Member _____
(Yong Wang, PhD)

Committee Member _____
(Burrell Montz, PhD)

Chair of the Department of Geography, Planning, and Environment

_____
(Jeff Popke, PhD)

Dean of the Graduate School _____
(Paul J. Gemperline, PhD)

DEDICATIONS

I would like to dedicate this manuscript to my parents and my partner, Elizabeth. This thesis could not have been completed without their endless support over the past two years. I cannot thank them enough for their continual encouragement throughout this whole process.

ACKNOWLEDGEMENTS

First and foremost, I would like to thank my advisor, Dr. Hannah Sirianni, for her support and guidance throughout my time at East Carolina University. The experiences and skills I have gained through her mentorship will be invaluable moving forward in my career. I would also like to thank my committee members, Dr. Thad Wasklewicz, Dr. Yong Wang, and Dr. Burrell Montz, for their support and feedback on this research. Lastly, I would like to thank Eric Diaddorio, of ECU's Dive and Water Safety team, as well as my lab mates for their valuable assistance out in the field.

TABLE OF CONTENTS

LIST OF TABLES

LIST OF FIGURES

CHAPTER 1: INTRODUCTION

Natural and anthropogenic factors are changing estuarine systems across the globe. Estuarine shorelines often erode at exceptionally high rates (Eulie et al., 2017) due to interactions between basin geometry as well as wind and wave climate (Lorang and Stanford, 1993; Hardaway and Gunn, 2010). These interactions are heightened as sea level rise intensifies and extreme storms become more frequent due to climate change. Further studies are needed to better understand how estuarine shorelines, and the communities along them, are changing in response to these complex factors. Shoreline classification maps are critical tool for understanding the context and magnitude of storm-induced erosion (Riggs and Ames, 2003). They enable coastal communities to better understand erosion risks associated with different shoreline environments and are a tool for monitoring natural and engineered changes along the shoreline. These maps also aid decision-makers such as coastal managers in mitigating erosional hazards.

Coastal North Carolina has experienced an increase in the frequency of extreme storms (Paerl et al., 2019), with over 36 tropical cyclones occurring since the late-1990s (Paerl et al., 2019). The Albemarle-Pamlico Estuarine System (APES), the second-largest estuarine complex in the United States, and its major tributaries are experiencing significant shoreline change in response to extreme storms and rising sea levels. A substantial portion of these extreme storms has impacted the Neuse River Estuary (NRE), a major tributary of the APES. Hurricane Bertha, in July 1996, produced a storm surge that raised water levels 2.0 to 2.4 meters above mean levels, causing localized bluff retreat of 0.1 to 1.5 m between Otter Creek and Slocum Creek. Hurricane Fran, in September 1996, caused an additional shoreline retreat of 3.0 to 12.0 m within the NRE (Phillips, 1999). In September 2018, Hurricane Florence brought storm-force waves that eroded east-facing

bluffs within the NRE, impacting hundreds of residences. The largest localized bluff retreat observed from this storm was above 20.0 m, significantly greater than the retreat observed during Hurricane Fran (Phillips, 1999; Phillips, 2022). The city of Havelock and town of Arapahoe, NC experienced storm surges on the NRE of 2.4 to 3.1 m above the Mean Higher High Water (MHHW) line (Stewart and Berg, 2019). Rates of erosion along the estuarine shorelines of North Carolina can be greater than that of oceanfront shores (Corbett et al., 2008; Cowart et al., 2011), with storm-generated forces posing a major threat. NRE shorelines are particularly prone to this type of erosion as these extreme storms become more frequent (Phillips, 1999; Paerl et al., 2019). No updated, high-resolution shoreline classification map currently exists for the NRE. Therefore, creating such a map will allow communities to better understand erosion risks within the estuary and support informed management of the NRE moving forward.

1.1 Previous Shoreline Mapping Efforts in the Neuse River Estuary

At the federal level, the National Oceanic and Atmospheric Administration (NOAA) has consistently produced estuarine shoreline maps over the past decade through the Coastal Change Analysis Program (C-CAP). C-CAP produced a regional land cover map of the NRE most recently in 2016 with 30 m resolution using Landsat Thematic Mapper imagery. C-CAP regional land cover maps span all coastal areas within the contiguous United States but feature a broader classification scheme that incorporates land cover types across the country. C-CAP regional land cover maps are helpful for detecting land cover change. Still, the coarse resolution of the maps does not allow for fine and accurate classification of estuarine types. The C-CAP classification process combines modeling, ancillary data, and hand-editing, which is both a labor-intensive and time-intensive

process. The C-CAP maps are produced to reach 85% overall accuracy, and NOAA aims to meet 80% accuracy per class, although this is not always achieved (McCombs et al., 2016).

At the state level, the most recent estuarine shoreline map of the NRE was produced in 2012 through the Estuarine Shoreline Mapping Project by the North Carolina Department of Coastal Management (NC DCM) and East Carolina University (ECU). This project used 6-inch resolution orthophotos from 2007, 2008, and 2010 and classified the shoreline via hand-editing and an extensive QA/QC process (McVerry, 2012). The classification scheme used for this map was based upon geomorphological characteristics and is comparable to the schemes used by Riggs and Ames (2003) and Corbett et al. (2008). The estuarine shoreline map had high accuracy due to hand-editing and the extensive QA/QC process, but this methodology is labor- and time-intensive. More efficient classification methods will allow the latest remote sensing data to be processed faster, providing coastal stakeholders with early access to critical decision-making tools.

Efforts to improve shoreline mapping within the APES, including the NRE, have been ongoing over the past two decades. Initial efforts focused on defining and mapping current shoreline classifications and quantifying shoreline change rates within the NRE (Corbett et al., 2008; Cowart et al., 2011). More recent efforts have shifted to digitizing the estuarine shoreline and investigating how land-use, land-cover, and stabilization structures correlate to shoreline change rate (Cowart et al., 2011; McVerry, 2012; Polk and Eulie, 2018).

There remains a gap in the existence of a current, high-resolution shoreline classification map of the NRE. Advanced digital image processing techniques, such as object-based segmentation and machine learning classification, should be explored to take advantage of the growing amount of high-resolution aerial imagery available to coastal stakeholders.

1.2 Pixel-Based vs. Object-Based Image Classification

Image classification in the context of remote sensing is the process of identifying cover types using the spectral information of an image. It serves as the basic framework for shoreline classification map development. A wide range of image classification techniques exist, but all techniques can be split into two major approaches: pixel-based and object-based classification. Pixel-based classification is the classification of an individual image pixel based upon extracted spectral information. Object-based classification, using a process known as Object-Based Image Analysis (OBIA), refers to the aggregation of image pixels into spectrally homogeneous objects (image segmentation) and the subsequent classification of these image-objects based on feature statistics (Liu and Xia, 2010). OBIA has emerged as a useful approach as objects provide contextual information and can better represent landforms than pixels (Townshend et al., 2000; Gercek et al., 2011; Martha et al., 2018; Cooper et al., 2019; Kotaridis and Lazaridou, 2021). OBIA is also known to reduce local noise and heterogeneity, as well as the uncertainty of positional discrepancy between imagery and *in-situ* data (Liu and Xia, 2010; Zhang et al., 2018). In principle, the approach is considered more transferable and reproducible than pixel-based classification (Hofmann et al., 2011). However, OBIA introduces the opportunity for additional error during the image segmentation process (Möller et al., 2007; Kampouraki et al., 2008; Liu and Xia, 2010). Both under- and over-segmentation can occur depending on imagery resolution, class characteristics, and input parameters, affecting the classification accuracy. Additionally, a past study comparing pixel-based and object-based classifications in an intertidal shoreline environment showed that some shore classes had higher classification accuracies through pixel-based classification (Demers et al., 2015).

Given the advantages, OBIA is anticipated to be the best approach for estuarine shoreline classification. However, a pixel-based classification should also be conducted to confirm this anticipation, given that neither approach has been used in the NRE prior to this study.

1.3 Machine learning (ML) in shoreline classification

Machine learning classification has emerged as a popular framework within remote sensing research over the past two decades (Foody et al., 2007; Mountrakis et al., 2011; Belgiu and Drăguţ, 2016; Maxwell et al., 2018). Machine learning classification algorithms are able to predict complex classes using a wide array of input training data without having to make any assumptions about the distribution of the data (Maxwell et al., 2018). There are many machine learning algorithms used for classifications, each with their pros and cons. For this reason, this study compares the ability of five machine learning algorithms to classify estuarine shorelines. These include random forest (RF), support vector machine (SVM), LibLINEAR (LL), artificial neural network (ANN), and *k*-nearest neighbors (*k*-NN).

RF is a supervised learning algorithm that uses an ensemble of decision trees to determine the final classification. RF is effective when applied to the classification of multi-source and hyperspectral data (Crawford et al., 2003, Ham et al., 2005, Gislason et al., 2006, Lawrence et al., 2006, Chan and Paelinckx, 2008). However, contradictory results exist on how sampling design impacts RF classification results (Belgiu and Drăguţ, 2016). Mellor et al. (2015) determined that RF is not sensitive to mislabeled training data while additional studies found that RF is sensitive to spatial autocorrelation of training classes and training sample proportions (Dalponte et al., 2013; Millard and Richardson, 2015).

SVM is a non-parametric and non-linear supervised learning algorithm that classifies data by determining a boundary that maximizes the separation between support vectors. SVM has been

shown to improve land cover classification from remote sensing datasets as it avoids classification noise through the use of a hyperplane (Mountrakis et al., 2011; Choung and Jo, 2017). A disadvantage of SVM is that when applied to remote sensing datasets, the choice of kernel function does not always provide an ideal SVM configuration (Mountrakis et al., 2011). Given its similarities to SVM, linear classification, through the LibLINEAR package (Fan et al., 2008), also has the potential to improve land cover classification.

ANN is another non-parametric learning algorithm that produces an output class by feeding weighted input layers or 'nodes' into an activation function. This is an iterative process where the weights of the input layers are modified, and modifications are either kept or discarded depending on if the overall classification is improved. A downside to ANN is the "black box" technique, where it becomes difficult to understand how classification decisions are made based upon input data (Qiu and Jensen, 2004; Szuster et al., 2011). Both SVM and ANN have produced 94.15% and 94.99% accuracies, respectively, for land cover and land use classification within tropical coastal zones (Szuster et al., 2011).

k-NN is a supervised learning algorithm that can classify an output by taking a majority from the *k*-nearest neighbors, where a user determines *k*. *k*-NN classification is advantageous because it produces spatially conscious predictions, but this involves a large number of calculations. When a sample is unbalanced, the model is more susceptible to misclassification (Wang et al., 2019). In a study regarding the land-cover classifications of coastal wetlands, *k*-NN produced an overall accuracy of 87.14% for Worldview-2 images (Wang et al., 2019). All five algorithms present different advantages and disadvantages to classifying an estuarine shoreline environment and have the potential to perform differently depending on training data and algorithm parameters. Therefore, all five algorithms are explored within this study.

In recent years, machine learning approaches to land cover classification have trended towards deep learning compared to other machine learning techniques (Vali et al., 2020; Zhang et al., 2020). Deep learning has proven successful in working with large, complex datasets but is relatively new in its application to remote sensing data. The five algorithms being explored in this study were chosen over newer deep learning approaches as there is documented success of their use in classifying a wide range of environments. As this study explores an object-based ensemble approach in a new estuarine environment, the use of algorithms with proven success in a variety of environments is key to maximizing the accuracy of the shoreline classification map.

1.4 Ensemble Analysis and Uncertainty Measures

An ensemble analysis is a classifier system that combines a diverse set of machine learning classifier outputs to improve overall classification (Du et al., 2012). The combined strength of the ensemble offsets the individual model variances and biases and improves the stability and predictive power of the model. The result is often better than the worst individual classifier used and generally more accurate than all individual classifiers (Liu et al., 2004; Foody et al., 2007). Several different methods combine the outputs from individual classifiers into a final ensemble classification. Two widely held methods are the majority vote and weighted vote (Kuncheva, 2004; Du et al., 2012; Zhang et al., 2016). In the former, the class that obtains the majority of votes is selected as the classification of the object. For the latter, the weight of each classifier is generated based upon a chosen attribute. A straightforward approach is to weigh each classifier based on the estimated accuracy of the training set (Du et al., 2012).

Another advantage of conducting an ensemble analysis is producing an uncertainty map. An uncertainty map presents the confidence of the model in predicting each object. This can be

used to distinguish locations within the study area where differentiating a class is difficult (Foody et al., 2007). Such information is useful when prioritizing future fieldwork locations and reducing overall classification error.

An ensemble approach has been successfully applied in terrestrial (Waske et al., 2009; Blaschke, 2010; Du et al., 2012), coastal (Zhang and Xie, 2014), and aquatic environments (Zhang, 2015). Combining an object-based ensemble framework has also been successfully used in vegetation classification (Zhang et al., 2016; Tonbul et al., 2020) but has yet to be applied to estuarine shoreline classification. Therefore, employing an ensemble analysis to classify the NRE shoreline should be valuable in maximizing the accuracy of the final estuarine shoreline classification map. The associated uncertainty map aids in the prioritization of future classification efforts within the NRE.

1.5 Shoreline Change and Vulnerability Assessment

A benefit to the object-based ensemble approach is resulting objects and classifications can be used in various shoreline management applications, including shoreline change analysis and assessment of shoreline vulnerability. Past efforts to quantify shoreline change within the NRE have captured long-term change rates from 1950s-1990s and short-term change rates from 2010-2011 (Corbett et al., 2008; Cowart et al., 2011; Eulie et al., 2017). In a historical assessment of shoreline change in the NRE, Corbett et al. (2008) and Cowart et al. (2011) used the end-point rate (EPR) method to calculate the mean annual shoreline change rate (SCR, m/yr) across a 40-year period from 1958-1998. Mean SCR refers to the distance of change between delineated shorelines divided by the time period to produce an average rate of change over time. The NRE shoreline was delineated from aerial photographs in 1958 and 1998 based on the wet/dry line of sediment

shorelines and vegetation boundary of vegetated shorelines (Corbett et al., 2008; Cowart et al., 2011). In a more recent assessment of shoreline change within the greater APES region, Eulie et al. (2017) quantified both long-term (historical) and short-term SCRs also using the end-point method and same shoreline delineation approach as Cowart et al. (2011). Long-term assessments spanned across 1950s-2006/2007 along with various subsets of this time period and short-term assessments spanned across June 2010-May 2011 along with three-month subsets. One advantage of the EPR method is the avoidance of a reference baseline, allowing for direct comparison between two different shoreline years. It also quantifies SCR without having to adjust or smooth the shoreline prior to analysis. Conversely, the EPR method is known to provide a conservative SCR estimate (Cowart et al., 2010) and this can oversimplify the complex morphodynamics of a given system.

No assessment of shoreline change has been conducted within the NRE since 2011. This lack of recent assessment introduces an opportunity to apply the object-based results to the shoreline delineation and SCR quantification from 2016 - 2020. The range of 2016-2020 was chosen to capture shoreline change pre- and post-Hurricane Florence (2018) and align with available aerial imagery from the United States Department of Agriculture (USDA) National Agriculture Imagery Program (NAIP). A goal is to determine if object-based ensemble results produce comparable findings. A potential advantage of applying object-based analysis results to assessing shoreline change is the approach provides both a shoreline delineation as well as corresponding shoreline classification. In past studies, Land-Use Land-Cover (LULC) classification has been considered for its effect on shoreline change within the NRE and change rates were found to have some variability related to the classification (Cowart et al., 2011). An

object-based approach to SCR can then be used to assess shoreline vulnerability, an assessment that has yet to be conducted at a local scale within the NRE.

Vulnerability assessments are used to characterize the susceptibility of a given system and estimate the potential damage that may result from hazardous events (Wisner et al., 2014). Many approaches exist for conducting vulnerability assessments, but one of the most well-known approaches in the coastal environment is the coastal vulnerability index (CVI) (Gornitz, 1990; Gornitz et al., 1994). CVI was initially created using seven physical variables to define coastal vulnerability on the East Coast related to sea-level rise (Eq. 1).

$$CVI = \frac{\sqrt{(a \times b \times c \times d \times e \times f \; x \; g)}}{7} \qquad (1)$$

Where a = Relief (m), b = Rock Type, c = Landform, d = Vertical Movement (RSL Change) (mm/yr), e = Shoreline Displacement (m/yr), f = Mean Tidal Range (m), and g = Maximum Wave Height (m).

Modifications to the original CVI have been introduced since its inception and have become widely used (Shaw et al., 1998; Thieler and Hammar-Klose, 1999; Lopez et al., 2016). The CVI and derivatives have been applied in a variety of coastal environments (Shaw et al., 1998; Thieler and Hammar-Klose, 1999; Pendleton et al., 2004: Boruff et al., 2005; Doukakis, 2005; Diez et al., 2007; Nageswara Rao et al., 2008; Ozyurt and Ergin, 2010; Abuodha and Woodroffe, 2010; Lopez et al., 2016; Koroglu et al., 2019) and provide an organized framework that is well known amongst coastal planners and managers. However, the set formula does not sufficiently consider data availability as well as the unique features of the study location that can also influence vulnerability (Bukvic et al., 2020). More recent approaches to CVI assessments have expanded to incorporate social and economic vulnerabilities as well as other physical variables (Palmer et al.,

2011; Balica et al., 2012; Mohamad et al., 2014; Kantamaneni et al., 2018; Ruzic et al., 2019; Bukvic et al., 2020), but still do not improve upon the rigidity of the framework.

Given the familiarity and adaptability of the CVI framework, it was applied in this study to assess shoreline erosion vulnerability within the NRE. Although recent CVI adaptations provide a more robust assessment of vulnerability by including socioeconomic vulnerability, an assessment of that scale goes beyond the scope of this study.

1.6 Objectives

This study is designed with the goal of assessing the ability of an object-based ensemble analysis framework to generate updated and accurate shoreline maps of the Neuse River Estuary (NRE). Here, *in-situ* reference data, LiDAR-derived elevation and intensity data, and high-resolution aerial imagery are used to train five machine learning algorithms to classify the NRE shoreline. The shoreline classification scheme is derived from previous classification efforts completed by Riggs and Ames (2003) and Corbett et al. (2008) and is refined in this study to incorporate slope and engineered modifications. Random Forest (RF), Support Vector Machine (SVM), LibLINEAR (LL), Artificial Neural Network (ANN), and k-Nearest Neighbors (k-NN), are assessed both individually and as a multiple classifier system (MCS) or ensemble analysis, for classification accuracy. Introducing machine learning classifiers and ensemble analysis within NRE shoreline classification methods has the potential to improve overall classification accuracy and efficiency while providing important context to coastal managers regarding shoreline erosion and coastal development. Specific objectives include: 1) to compare five machine learning algorithms, RF, SVM, LibLINEAR, *k*-NN, and ANN, to determine which is best suited for classifying the NRE shoreline; 2) to evaluate and explore the effectiveness of an object-based

ensemble approach in classifying shoreline types within the NRE; and 3) to account for the effects of uncertainty within the final shoreline classifications and map where object-based uncertainty is present.

An additional objective of this study is to illustrate how an object-based ensemble approach can be used in future shoreline management of the NRE. Quantifying shoreline change and assessing shoreline vulnerability is a vital part of shoreline management and is therefore chosen as an example application. More complex and precise approaches to assessing shoreline change and shoreline vulnerability exist for estuarine shoreline environments. However, these approaches fall beyond the scope of the study and have the potential to be explored in future work.

CHAPTER 2: STUDY AREA AND DATA

2.1 Study Area

The study takes place along the NRE shoreline in North Carolina (Figure 1). The NRE is a major sub-estuary of the Albemarle-Pamlico Estuarine System (APES) and flows through Craven, Carteret, and Pamlico counties before emptying into the Pamlico Sound. The Neuse River feeds into the NRE with an average annual discharge of 183 m^3 s^{-1}, providing a large volume of freshwater flow into the Pamlico Sound (Cowart et al., 2011; U.S. Geological Survey, 2020). The area was selected as it is representative of the geographic conditions of the greater APES region, including the shoreline orientation, wind and wave energy, relative location, and erosional rate. The NRE has low tidal influence, as it is separated from the Atlantic Ocean by the Outer Banks barrier islands but is subject to a dynamic range of physical energy conditions, including storm-driven waves and high winds (Cowart et al. 2011). The NRE also has a high density of development along the coastline and offers numerous ecosystem services to the APES, including filtration of excess nutrients and pollution (Day et al., 1989; Martin et al., 1996; Crossett et al., 2004). The NRE is subject to natural and anthropogenic processes, with severe weather events, sea-level rise, boat wakes, and urban development as known aggravates of erosion (Polk and Eulie, 2018).

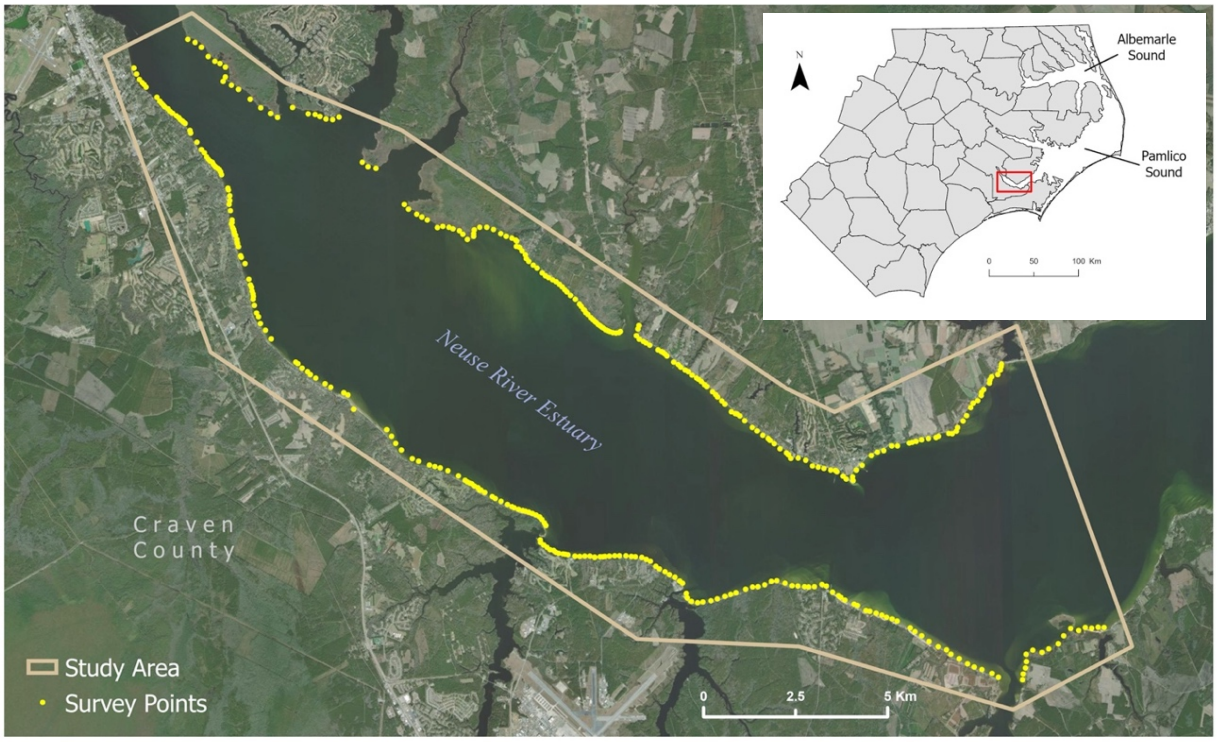

Figure 1. A map illustrating the designated study area and survey points within the Neuse River Estuary, NC. The red box within the insert map indicates the location of the Neuse River Estuary in relation to the Albemarle and Pamlico Sounds in eastern North Carolina.

2.2 Data

2.2.1 In-situ Estuarine Shoreline Data Collection

In-situ reference data were collected for this study to evaluate the shoreline classification (Figure 1). The shoreline classification scheme derived from previous classifications (Riggs and Ames, 2003; Corbett et al., 2008) has been refined for this study to incorporate modified or engineered structures (Table 1). The *in-situ* data were collected onboard a vessel to survey the entire length of coastline within the study area. An iPad with the ESRI application ArcGIS Survey123 software (http://www.esri.com/) was used for logging data points on the vessel and recording the associated shoreline classification along with the latitude and longitude of the vessel. The date and time for each data point were also recorded within the application. A laser rangefinder and compass were used to extrapolate the exact location of the shoreline by recording the distance

in meters from boat to shoreline and the angle (degrees) of the distance measurement. A Sony R7R III Camera was then used to capture imagery of each shoreline type, and the image number was logged with each data point. Three hundred ninety-five data points were captured within the survey area over four field days.

Initially, the modified shoreline classification was split into two sub-classes, modified vertical shoreline (ex. bulkhead, seawall) and modified sloped shoreline (ex. rip-rap). This division would provide a more detailed characterization of the modified structures present in the NRE as well as insight to how these structures correlate with erosion rates, given the complex morphodynamics of the NRE. However, statistically significant sample sizes of the two sub-classes were not able to be obtained in the field and the two sub-classes were consolidated into one modified shoreline classification.

Table 1. Shoreline classification scheme modified from previous classification efforts completed by Riggs and Ames (2003) and Corbett et al. (2008).

Shoreline Category	Shoreline Sub-Category	Description
Sediment Bank	Low Sediment Bank	Less than 1.5 m
	High Sediment Bank	1.5 m to 6.1 m
	Natural Bluff	Greater than 6.1 m
Organic	Marsh	Fresh, brackish, & salt waters
	Swamp Forest	Freshwater riverine floodplain
Modified	Modified	Non-natural shoreline (Ex.: Rip-rap, bulkhead, seawall)

2.2.2 Remote Sensing Data

Aerial imagery was used to divide the captured images into vector objects. The most recent aerial imagery was collected in 2020 by the USDA NAIP as natural color and color infrared compressed county mosaics (CCMs) with 0.6-meter resolution. Earlier imagery was not used in

the object-based ensemble analysis as the aim was to create an updated shoreline classification map for 2020.

LiDAR all return point data and LiDAR intensity data were also used to classify imagery and have 0.7 m nominal pulse spacing, respective of spring 2014 collection. LiDAR was collected by the NOAA Office of Coastal Management (OCM) and North Carolina Floodplain Mapping Program (NCFMP) using a Leica ALS70 LiDAR system, with 0.063 m vertical error and 1.0 m horizontal error. The rasterization of the LiDAR point cloud to a DEM was completed with binning interpolation using a minimum value. 2014 LiDAR was the most recent LiDAR dataset available for the given study area when this analysis took place.

Some studies have shown that LiDAR intensity data, when combined with LiDAR elevation, can improve land cover classification (Brennan and Webster, 2006; Antonarakis et al., 2008) but images derived from the returned laser intensity can appear heterogeneous and speckled (Flood, 2001; Kaasalainen et al., 2005; Maxwell et al., 2015). This is due to the wide range of factors that impact the returned laser intensity including angle of reflectance, collection range, roughness, moisture, and surface composition. Therefore, LiDAR intensity data was inspected prior to inclusion in the overall mapping framework and it was determined that no calibration and smoothing tools would be applied. The NOAA Data Access Viewer was used to obtain remotely sensed data (https://coast.noaa.gov/dataviewer/)

CHAPTER 3: METHODOLOGY

A framework was designed to evaluate the ability of an object-based machine learning classifier ensemble approach to generate accurate shoreline maps of the NRE (Figure 2). The first step in this framework was to use image segmentation to produce image objects from spectral imagery. The objects created from this segmentation were then matched with four additional parameters, LiDAR elevation, LiDAR intensity, Normalized Difference Vegetation Index (NDVI), and slope, as well as *in-situ* reference data in order to create a matched dataset. Five machine learning algorithms, RF, SVM, LibLINEAR, *k*-NN, and ANN, were trained on this dataset and the outcome and accuracy of each algorithm informed the outcome determined by the ensemble analysis. The results of this framework were compared against a pixel-based approach to determine if an object-based methodology improves classification within an estuarine shoreline environment. An estuarine shoreline classification map and corresponding uncertainty map were produced from the object-based ensemble analysis.

The image objects resulting from this framework were then used to delineate a 2020 shoreline and were compared against 2016 and 2018 shorelines also derived from image objects. EPR methodology was applied to calculate shoreline change within the 4-year period and subsequently combined with 2020 shoreline classifications and slope (%) to assess overall shoreline vulnerability.

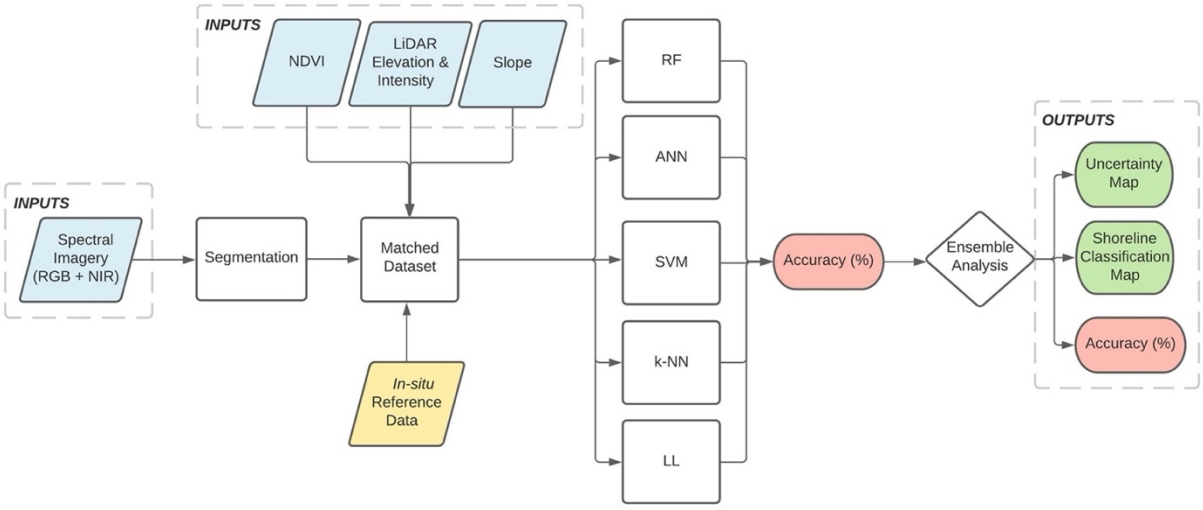

Figure 2. Framework for object-based ensemble analysis where RF = Random Forest, ANN = Artificial Neural Network, SVM = Support Vector Machine, k- NN = K-nearest neighbor, and LL = LibLINEAR.

3.1 Image Segmentation

A multi-resolution image segmentation algorithm in eCognition Developer software was used (Benz et al., 2004; Trimble, 2018) to conduct the object-based approach for image classification. The segmentation algorithm divides spectral imagery into pixel segments and merges adjacent segments based on a relative homogeneity threshold to create vector objects (Benz et al., 2004; Trimble, 2008). The threshold was determined by the following input parameters: scale, color/shape, and smoothness/compactness. Scale is the maximum standard deviation of the homogeneity threshold and determines the size of objects. Larger-scale values result in larger heterogeneous objects, and smaller-scale values result in smaller homogeneous objects (Cooper et al., 2019). Scale values between 20 and 40 were tested to identify an optimal scale for defining shoreline classifications. This range has been successfully used in a past study that applied object-based image analysis to remotely sensed data of a similar resolution (Cooper et al., 2019). A scale value of 25 was chosen as it produced the largest, homogeneous objects. Color represents the digital value of the pixel and shape defines the textural homogeneity of the image objects by

totaling smoothness and compactness. Smoothness optimizes objects by how similar the shape is to a square, while compactness optimizes objects by how similar the pixel cluster is to a circle. The color/shape and smoothness/compactness parameters sum to a weighted value of 1. For this framework, the color/shape parameter was set to 0.2/0.8 for all bands, respectively, so that more weight is given to the object's geometry. Smoothness/compactness was set to 0.5/0.5 for all bands so that equal weight is given to compact and non-compact segments.

In-situ reference data were then spatially matched with the vector objects. Image segmentation was omitted for the comparative pixel-based approach and *in-situ* reference data was simply matched with individual pixels. These matched datasets were then applied to the five machine learning classifiers being assessed within this study.

3.2 Training, Validating, and Testing the Machine Learning Classifiers

Training of the RF, SVM, LibLINEAR, *k*-NN, and ANN classifiers was conducted using Waikato Environment for Knowledge Analysis (Weka, Version 3.8.4), an open-source data mining software (Hall et al., 2009; Frank et al., 2016). The predictors and parameters for each classifier were fine-tuned using trial-and-error, and the *k*-fold cross-validation method, where k=10, was used to train each machine learning classifier (Maxwell et al., 2018). In the RF classifier, maximum tree depth has the most influence on overall prediction accuracy. In the SVM algorithm, four kernel-based methods were tested: linear, sigmoidal, radial basis function (RBF), and polynomial kernels. A linear kernel-based method produced higher overall accuracies than sigmoidal, RBF, and polynomial kernel-based methods, and was selected as a final parameter. For the LibLINEAR classifier, the optimal SVM type was L2-regularized L2-loss SVC (primal), with bias and cost values set at 2.0. For *k*-NN, a value of $k=3$ was specified based upon the chosen number of user-

defined training objects. In the ANN classifier, the learning rate was defined as 0.5 and number of hidden layers as 0. A full list of parameters specifications can be found in APPENDIX A.

3.3 Ensemble Analysis and Uncertainty Mapping

An ensemble analysis was conducted from the outputs of RF, SVM, LibLINEAR, *k*-NN, and ANN. A combination of the majority vote and weighted vote was used to determine the final output classification (Zhang et al., 2015) (APPENDIX B). If the majority of the five classifiers choose the same class, the object was assigned that class. If all five classifiers chose a different class, a weighted vote was used and the classifier with the highest accuracy was assigned a weight of 1 with all other classifiers assigned a weight of 0. In the case of a tie (e.g., SVM and RF vote class 1, *k*-NN and ANN vote class 2, and LibLINEAR votes for class 3), the class that has the highest summed accuracy between the two classifiers was chosen. The accuracy of the ensemble was compared to the individual classifiers using overall accuracy, user's accuracy, and producer's accuracy. User's accuracy measures errors of commission or the likelihood that the map classification agrees with the real-world classification. Producer's accuracy measures errors of omission or the likelihood that real-world classes are correct on the map produced.

An uncertainty map was derived from the ensemble analysis classification results if the ensemble produced a higher overall accuracy than individual classifiers. The map illustrated either complete agreement, partial agreement, or no agreement between classifiers. Complete agreement resulted from a unanimous vote, partial agreement from a majority vote that is not unanimous or a tied vote, and no agreement resulted from each classifier voting differently.

3.4 Calculating Error Matrix and Kappa Statistic

A standard approach to accuracy assessments in remote sensing is the use of an error matrix and Kappa statistic (Congalton and Green, 2009). An error matrix was produced from the final classifications for both object-based and pixel-based methods. The Kappa statistic was also derived from the error matrix and a value greater than 0.80 indicated strong accuracy (Landis and Koch, 1977).

3.5 Shoreline Change and Vulnerability Assessment

With high-resolution NAIP imagery available from 2016, 2018, and 2020, an assessment of both pre-Hurricane Florence (2016-2018) and post-Hurricane Florence (2018-2020) shoreline change was conducted. Image objects created using the above object-based ensemble workflow were then used to delineate the 2020 shoreline. Using ArcGIS Pro version 2.6 (http://www.esri.com/), objects were merged and converted from polygons to polylines. The polylines were then edited to remove portions not bordering the water, and the remaining portions were used as the delineated shoreline. The multi-resolution segmentation algorithm in eCognition software was applied to create image objects for 2016 and 2018 NAIP imagery. Image objects were then brought into ArcGIS Pro and followed the same delineation process as the 2020 shoreline.

Previous quantifications of shoreline change in the NRE (Cowart et al., 2011; Eulie et al., 2017) successfully employed the EPR methodology conducted by Cowart et al. (2010) to calculate a mean annual SCR (m/yr). The EPR methodology was adopted in this study to calculate SCR from 2016-2020 and allow for direct comparisons of SCRs over time. However, context was

provided on if observed rates aligned with shoreline changes observed in the field following Hurricane Florence.

Similar to Cowart et al. (2010), the Generate Points Along Lines tool (Data Management Toolbox) was used to create reference points every 50 m along the 2018 shoreline (*n=1946*). The Near Tool within the Proximity Analysis Toolbox was then used to calculate the nearest distance between these 2018 reference points and the 2016 and 2020 shorelines. The intersection of 2018 reference points with 2016 and 2020 image objects was used to determine if the calculated shoreline change was erosional or depositional. Mean annual SCR (m/yr) over 2016-2020 was calculated by dividing the sum of the shoreline change by 4 years. A spatial join was then used to link 2018 reference points with the nearest 2020 image object in order to combine object attributes, including shoreline class and slope, with the mean annual SCR.

The modified CVI framework created by Thieler and Hammar-Klose (1999) was adapted to assess shoreline erosion vulnerability in this study. Given the scope of this study, three of the six physical variables were selected for use in the assessment including geomorphology (here shoreline class is used), slope (%) and shoreline erosion/accretion (m/yr) (Table 2) (Eq. 2).

Table 2. Ranking of coastal vulnerability index (CVI) risk variables included in the assessment.

	Ranking of Coastal Vulnerability Index				
	Very Low	**Low**	**Moderate**	**High**	**Very High**
VARIABLE	**1**	**2**	**3**	**4**	**5**
Shoreline Class	Swamp Forest	High Sediment Bank	Natural Bluff	Modified Shoreline	Marsh, Low Sediment Bank
Coastal Slope (%)	< 3.0	3.0 - 6.0	6.0 - 9.0	9.0 - 12.0	12.0 <
Shoreline Erosion/Accretion (m/yr)	> 2.0	1.0 - 2.0	-1.0 - 1.0	-1.0 - -2.0	< -2.0

$$CVI = \frac{\sqrt{(a \times b \times c)}}{3} \qquad (2)$$

where a = Shoreline Class, b = Shoreline Slope (%), and c = Shoreline Erosion/Accretion (m/yr).

Shoreline classes were ranked based upon previously documented levels of susceptibility to erosion in the NRE (Riggs and Ames, 2003; Corbett et al., 2008). The variable of coastal slope (%) was modified in this study to represent terrestrial slope up to the wet/dry line instead of both terrestrial slope and near-shore bathymetric slope. This modification was completed as terrestrial slope was an important predictor of the object-based ensemble analysis. The ranking of slope ranges was also reversed as this CVI aims to predict shoreline vulnerability to erosion rather than sea-level rise. Additionally, previous coastal slope rankings did not fully consider the susceptibility of sloped shorelines at or above 90° to base undercutting and subsequent collapse, which has been documented in the NRE. Shoreline erosion/accretion was defined by the variable rankings used by Thieler and Hammar-Klose (1999) as these matched the broad range of shoreline changes observed in the NRE. Quintiles of the CVI values were then calculated to define the 5 vulnerability categories: very low, low, moderate, high, and very high.

CHAPTER 4: RESULTS

4.1 Estuarine Shoreline Classification

The object-based ensemble performed best compared to all five individual algorithms. However, accuracy improvement between the ensemble and the next highest individual algorithm, the ANN classifier, was minimal (Table 3a). Regarding the user's accuracy, the ANN classifier produced the highest accuracy for the modified shoreline class, and the SVM algorithm produced the highest accuracy for the natural bluff shoreline class (APPENDIX C). The ensemble had the highest accuracies for high sediment bank, low sediment bank, swamp forest, and marsh shoreline classes (Table 4).

Table 3a-b. Overall accuracies and kappa values for (a) object-based and (b) pixel-based approaches by algorithm.

a. Object-based			b. Pixel-based		
Algorithm	Overall Accuracy (%)	Kappa Value	Algorithm	Overall Accuracy (%)	Kappa Value
RF	74.3	0.63	RF	70.1	0.57
kNN	69.2	0.57	kNN	64.3	0.5
SVM	72.2	0.61	SVM	65.3	0.5
LL	74.3	0.64	LL	64.3	0.49
ANN	75.1	0.65	ANN	65.6	0.51
Ensemble	76.4	0.66	Ensemble	69.1	0.56

Table 4. Error matrix for the object-based ensemble results by shoreline class.

Shoreline Classification	Modified Shoreline	Natural Bluff	High Sediment Bank	Low Sediment Bank	Swamp Forest	Marsh	Total	Producer's Accuracy (%)
Modified Shoreline	141	14	0	11	1	1	168	83.9%
Natural Bluff	21	42	0	1	0	0	64	65.6%
High Sediment Bank	8	1	1	1	1	0	12	8.3%
Low Sediment Bank	12	1	0	57	0	6	76	75.0%
Swamp Forest	7	0	0	1	3	3	14	21.4%
Marsh	1	0	0	1	0	53	55	96.4%
Total	190	58	1	72	5	63	Overall Accuracy:	
User's Accuracy (%)	74.2%	72.4%	100.0%	79.2%	60.0%	84.1%	76.4%	

No algorithm consistently produced the highest accuracy in each class regarding the producer's accuracy (APPENDIX C). The LibLINEAR algorithm produced the highest accuracy for the high sediment bank class, the RF classifier produced the highest accuracy for the marsh class, and the ANN approach produced the highest accuracy for the natural bluff and swamp forest classes. The ensemble procedure produced the highest for the modified shoreline class (Table 4). The RF, SVM, and ensemble algorithms are tied with the highest accuracy for the low sediment bank class at 75%. This lack of consistency in high accuracies across all shoreline classes supports the inclusion of the ensemble analysis in this study. Kappa values for the ensemble and all algorithms, aside from the kNN classifier, were within an interpretation of 'substantial' agreement per Landis and Koch (1977). The object-based ensemble accuracy was 6.3% higher than the top pixel-based model, RF (Table 3a, b). Kappa values for the pixel-based approach fell within a range of moderate agreement (Landis and Koch, 1977). Across both user's and producer's perspectives in both approaches, high sediment bank and swamp forest classes had low accuracy values (Table 4, 5). A non-parametric McNemar test was conducted (Foody, 2004) on both object-based and pixel-based results with a 95% confidence interval (z-score > 1.96) because of the minimal improvement of overall accuracy in the ensemble from the highest individual algorithm. In the object-based comparison of ANN and ensemble, there was no significant difference in classification accuracy (z-score = 1.0) A significant difference was seen in the pixel-based results of RF and ensemble accuracies (z-score = 5.7). The object-based ensemble was chosen to create the estuarine shoreline map for the Neuse River Estuary due to higher class accuracies for the majority of both user's and producer's perspectives compared to the object-based ANN model (Table 4, APPENDIX C). Classification results from the object-based ensemble analysis were placed over 2020 NAIP imagery to create the shoreline classification map (Figure 3a-d).

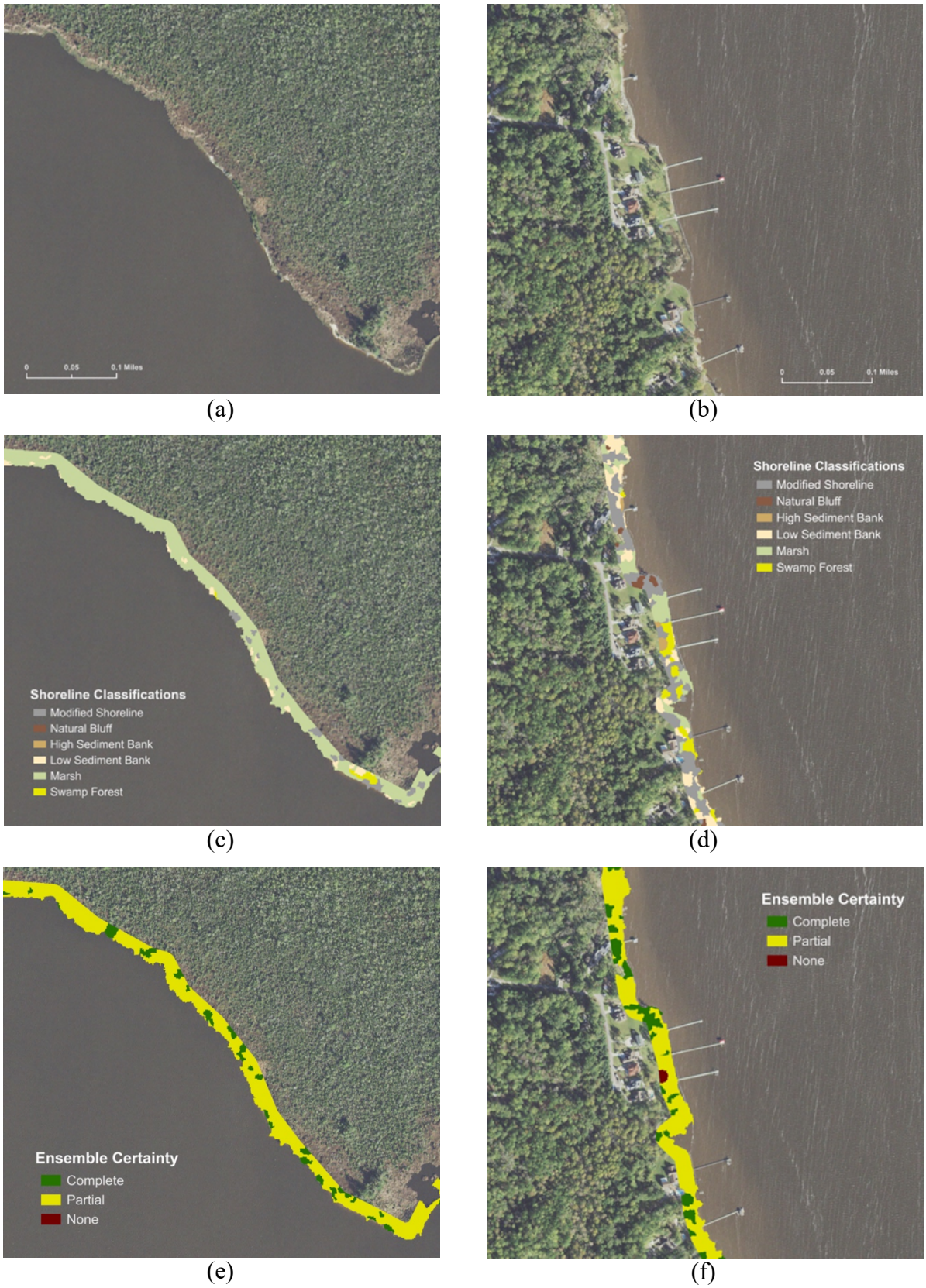

Figure 3a-f. (a-b) 2020 NAIP imagery of the north (a) and south (b) shore of the Neuse River Estuary overlayed with (c-d) shoreline classification and (e-f) ensemble certainty results from the object-based ensemble analysis.

Table 5. Error matrix for the pixel-based Random Forest (RF) results by shoreline class.

Shoreline Classification	Modified Shoreline	Natural Bluff	High Sediment Bank	Low Sediment Bank	Swamp Forest	Marsh	Total	Producer's Accuracy (%)
Modified Shoreline	139	9	0	13	3	6	170	81.8%
Natural Bluff	27	36	1	0	0	0	64	56.3%
High Sediment Bank	6	4	0	2	0	0	12	0.0%
Low Sediment Bank	16	1	0	53	0	8	78	67.9%
Swamp Forest	6	1	0	4	0	3	14	0.0%
Marsh	2	0	0	6	0	49	57	86.0%
Total	196	51	1	78	3	66	Overall Accuracy:	
User's Accuracy (%)	70.9%	70.6%	0.0%	67.9%	0.0%	74.2%	70.1%	

Most identified shoreline classes within the object-based ensemble were modified shorelines (Figure 4). This model shows a significant increase in percentage of modified shoreline compared to the 32.2% observed by Corbett et al. (2008) and approximately a 3% increase in modified shoreline from the classification conducted by McVerry in partnership with NC DCM and ECU (2012). A 7% decrease in sediment bank shoreline was also observed compared to the classification by McVerry (2012).

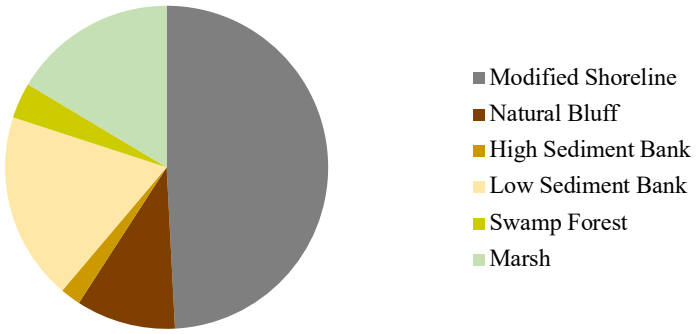

Figure 4. Distribution of shoreline classifications identified within the object-based ensemble model.

An assessment of uncertainty was conducted from the object-based ensemble model (Figure 3e, 3f). Complete certainty was seen in 31.8% of objects, partial certainty in 68.1%, and no certainty in 0.2%. The largest proportion of certainty was seen within modified shoreline and low sediment bank classes (Figure 5a, 5d). Consistent with accuracies observed in error matrices, high sediment bank and swamp forest classes had the largest proportion of no certainty amongst all classes, with 3.4% and 2.8% of objects respectively (Figure 5c, 5e).

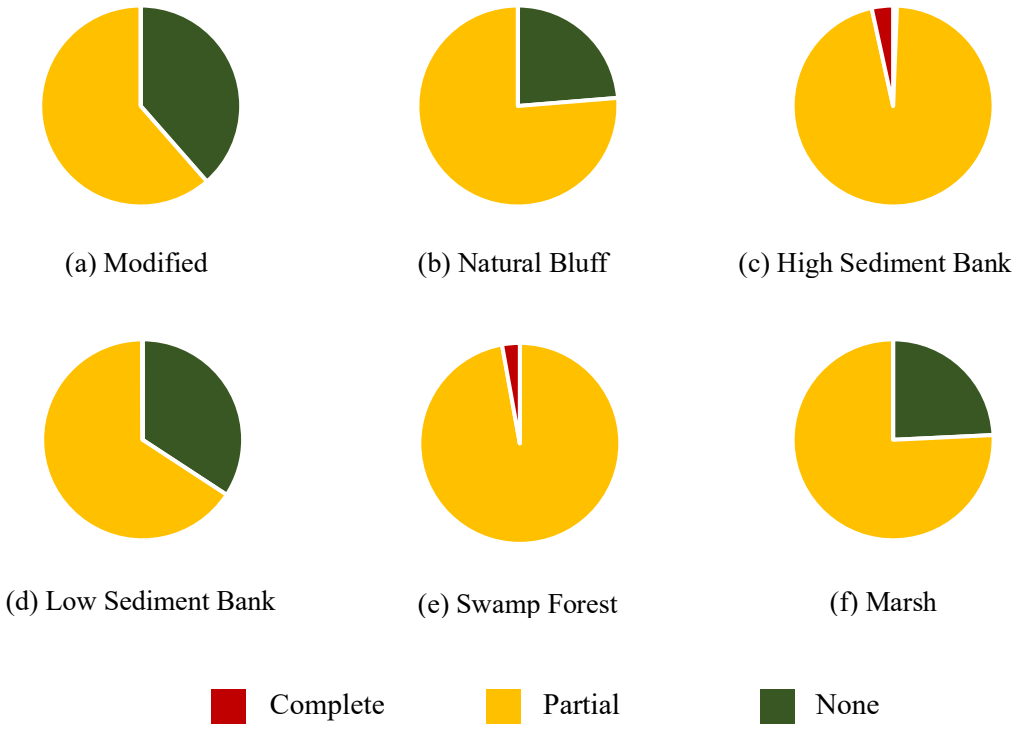

Figure 5a-f. Distribution of object uncertainty by shoreline class within the object-based ensemble.

4.2 Shoreline Change and Vulnerability Assessment

From 2016 to 2020, approximately 76% of the NRE shoreline eroded, 22% accreted, and 2% remained the same. The mean annual SCR (m/yr) of -0.55 m/yr was observed across the designated study area (Table 6, 7). The lowest mean SCRs and mean net shoreline changes were

seen in modified shoreline and natural bluff shoreline classes and the highest in low sediment bank and high sediment bank classes. Higher mean SCRs and mean net shoreline change were seen along the south shore of the NRE, although not significantly different from the north shore (Table 7).

Table 6. Mean shoreline change rate (SCR) and mean net change (2016-2020) results of individual and all shoreline classifications in the NRE.

Shoreline Classification	Mean SCR (m/yr)	Std. Dev.	Mean Net Change (m) (2016-2020)	Std. Dev.
Modified Shoreline	-0.46	0.92	-1.83	3.70
Natural Bluff	-0.49	1.08	-1.98	4.33
High Sediment Bank	-0.66	1.17	-2.62	4.70
Low Sediment Bank	-0.78	1.12	-3.10	4.49
Swamp Forest	-0.59	0.79	-2.38	3.16
Marsh	-0.56	0.99	-2.25	3.94
All Classes	-0.55	0.99	-2.18	3.95

Table 7. Mean shoreline change rate (SCR) and mean net change (2016-2020) results based on shoreline orientation within the NRE.

Shoreline Orientation	Mean SCR (m/yr)	Std. Dev.	Mean Net Change (m) (2016-2020)	Std. Dev.
North Shore	-0.48	0.80	-1.90	3.21
South Shore	-0.60	1.11	-2.40	4.43
All Shore Orientations	-0.55	0.99	-2.18	3.95

Across all shoreline classes, 45% of the NRE shoreline is highly or very highly vulnerable and 41% has low or very low vulnerability (Figure 6). Swamp forest and high sediment bank classes had the largest percentage of very low and low vulnerability rankings among the respective classes. Low sediment bank had the largest percentage of high and very high vulnerability with 64% of sampled points along the shoreline falling under these two rankings (Figure 6).

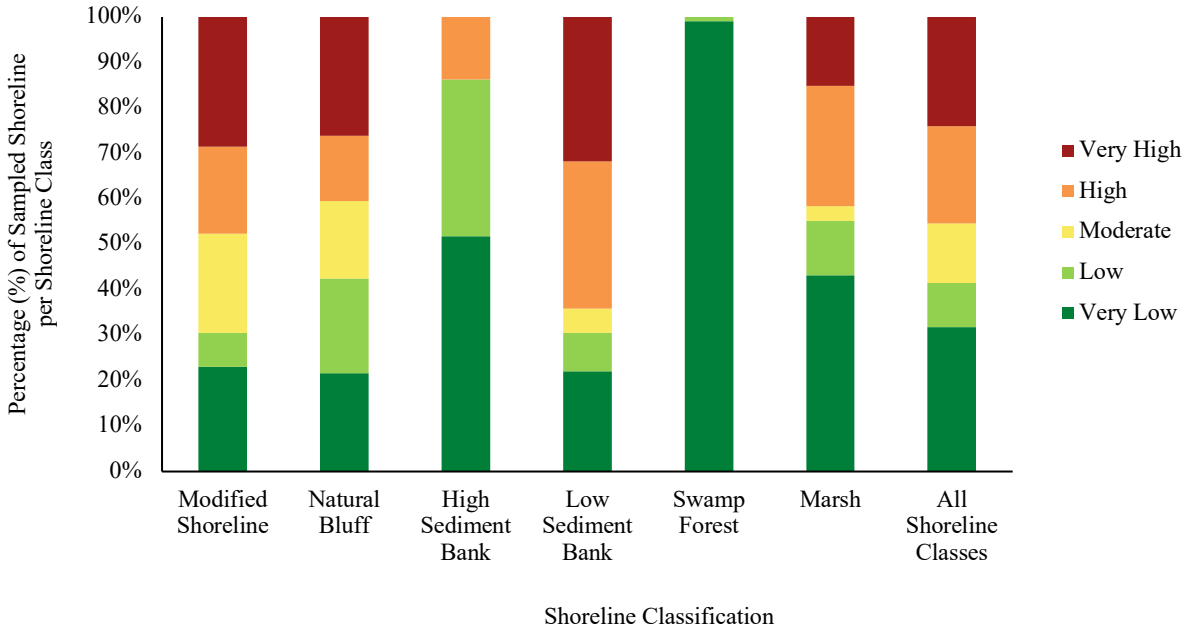

Figure 6. Distribution (%) of vulnerability rankings within individual and all shoreline classes based on CVI assessment of the NRE.

CHAPTER 5. DISCUSSION

5.1 Object-Based Ensemble Performance

The overall accuracy of the object-based ensemble model (76.4%) was 6.3% higher than the RF pixel-based model (70.1%), and higher user's and producer's accuracies were observed across all shoreline classes (Table 4, 5). Other coastal land classification studies that used different predictors or classification methodologies (McCarthy and Hall, 2013; Demers et al., 2015; Juel et al., 2015) produced overall accuracies between 63.3% to 92.1%. The object-based ensemble approach created and applied by Zhang et al. (2016) for classifying inland vegetation in the Florida Everglades produced an overall accuracy of 91.1%. The results from this study fall within the expected range of accuracy for remote sensing coastal classification but falls below the potential accuracy possible for the object-based ensemble methodology as a whole. This illustrates that the object-based ensemble approach is a viable way of classifying an estuarine shoreline environment such as the NRE but improvements are needed to maximize the full potential of the model. These improvements are discussed in subsequent sub-sections of this study.

5.2 Misclassifications

The largest percentage of misclassifications occurred within the high sediment bank and swamp forest classes (Table 4). These classes also saw highest percentage of total uncertainty in the ensemble model (Figure 5c, 5e). Both classes made up a combined 5% of the *in-situ* reference data collected for this study. Rogers and Skrabal (2001) and Riggs and Ames (2003) saw high sediment bank and swamp forest class abundance as <6% of the Neuse River. Although the percentage of reference data classes is comparable to these studies, the smaller sample size does

limit the range of spectral and elevation values collected for the two respective classes. High sediment bank misclassifications would also improve through the addition of a more recent LiDAR dataset for the NRE. The specific bank height range of the high sediment bank class, 1.5 m to 6.1 m, requires the most accurate LiDAR elevation data available in order to make accurate class predictions. Therefore, the use of a 2014 LiDAR dataset limits the accuracy to which this class can be identified within this study. It should be noted that in March 2022, a 2019-2020 NOAA National Geodetic Survey (NGS) Topobathy LiDAR dataset was published with point-spacing of 0.2 m but was not possible to incorporate into this study given time constraints. This new dataset should be incorporated into future studies within the NRE.

Over 15% of natural bluff and low sediment bank classes were misclassified as modified shoreline within the ensemble model. The wide spectral range of the modified shore class objects had significant overlap between the wide spectral range of the low sediment bank. The wide spectral range of the low sediment bank may be attributed to the variety of low sediment bank sub-classes that fall under this class (e.g., beach, low sediment bank with tree stumps, low sediment bank with marsh fringe, etc.). Separating a beach sub-class from the low sediment bank has the potential to improve classifications for both low sediment bank and modified shoreline classes. Separating other low sediment bank sub-classes may improve overall classification as well. Misclassifications of natural bluff shorelines as modified shorelines may be attributed to the wide LiDAR elevation ranges observed in the modified shoreline class. Vertical modified shorelines such as bulkheads and seawalls feature similar elevation characteristics as high sediment bank and natural bluff shorelines (i.e., presence of a vertical or near-vertical slope), especially when these modified structures are set back from the land/water interface.

5.3 Sources of Error and Limitations

There are two main sources of error that contribute to the class specific and overall accuracies observed in the object-based ensemble model. First, the differing spatial resolutions of the aerial imagery (0.6 m resolution) and LiDAR dataset (0.7 m pulse spacing) forced aerial imagery to be resampled in order to match the LiDAR dataset. Point spacing of LiDAR ground-return points, as classified by vendor, was calculated as 2 m, therefore aerial imagery was resampled to this same resolution. Through this resampling, finer spatial detail was lost and likely contributed to reduced accuracies of all shoreline class types.

A second main source of error was noted in the collection times of remotely sensed and *in-situ* datasets. 2020 NAIP imagery was collected in September and October 2020 and aligned with *in-situ* reference data collection that occurred between September and November 2020. The most recent LiDAR dataset available for the NRE was from spring 2014 collection. This significant time gap was both a limitation and source of error within the study. Given the number of storm events that occurred in the NRE between 2014 and 2020, the 2014 LiDAR collection likely included outdated elevation measurements that added to the probable error within the shoreline class predictions. However, a LiDAR dataset was necessary to distinguish between natural bluff, high sediment bank, and low sediment bank classes and the inclusion of the 2014 collection did improve both overall and individual class accuracies within the object-based ensemble model. Despite the potential error introduced by including the outdated LiDAR collection, it was still a necessary inclusion to produce the highest model accuracy possible.

5.4 Shoreline Change and Vulnerability Assessment

The EPR method and resulting rates of change are simple to calculate and have been widely used in past studies of erosion in the NRE. The -0.55 m/yr mean SCR (SD: ± 0.99 m/yr) observed across the NRE is comparable to past calculations of mean SCR at -0.58 m/yr (SD: ± 0.54 m/yr) over a 40-year period (Corbett et al., 2008; Cowart et al., 2011). However, given the significant erosion that was observed during Hurricane Florence, the -0.55 m/yr mean SCR calculated in this study is extremely conservative and does not align with the significant shoreline changes observed in the field. Shoreline change in the NRE is episodic in nature, with storm-driven dynamics largely influencing this change. Reducing shoreline change to an average rate per year oversimplifies and misrepresents the complex morphodynamics at play during these extreme storms. An initial study of Hurricane Florence's impacts on the NRE measured average bluff retreat at 11 m (Phillips, 2022). In this study, the lowest mean SCRs and mean net shoreline changes were seen in modified shoreline and natural bluff shoreline classes (Table 6). The significant bluff retreat observed during Hurricane Florence is not captured within this methodology when bluff erosion occurs inland behind a low sediment bank. Additionally, the mean SCR only represents a 2D change rate, rather than a 3D rate, which would likely provide a more accurate quantification the erosion observed along natural bluff and high sediment bank shorelines. Although past literature supports the use of the EPR methodology and associated change rates, in this study they provide an oversimplified quantification that should not be used without additional context or conversely, calculated through a different approach altogether.

The vulnerability assessment conducted does well at providing a base assessment of erosion risk within the NRE. The high proportions of high and very high vulnerability observed in the low sediment bank class align with the higher rates of erosion seen in both mean annual SCR

and net shoreline change from 2016-2020. A similar alignment is seen in the high proportion of low and very low vulnerability observed in the swamp forest class. This current assessment can be built on in future studies by refining current CVI variables, including improving the shoreline change quantification to incorporate NRE morphodynamics, and adding new physical and socioeconomic variables such as fetch, wave energy, mean tide range, economic value of property, and population. However, the approach shown in this study provides a valid example of how object-based ensemble results can inform an assessment of shoreline vulnerability and aid coastal managers in future shoreline management.

5.5 Future Avenues and Applications

The object-based ensemble analysis produced a high-resolution estuarine shoreline map that will aid coastal managers and other stakeholders in future shoreline management. In addition to the creation of additional sub-classes and incorporation of newer LiDAR data, another future avenue of this study would be to recreate the object-based ensemble workflow using entirely open-source software. With marked improvements over the past decade, QGIS and Orfeo ToolBox have the potential to produce similar OBIA results to ESRI ArcGIS Pro and eCognition. An open-source workflow would remove additional access barriers for coastal managers and allow for more frequent assessments of shoreline characterizations in the NRE.

Deep learning should also be explored in future classification studies within the NRE. As the volume of remote sensing data continues to grow at a remarkable pace, deep learning is a promising approach due to the success shown in working with large, complex datasets. Deep learning networks, especially convolutional neural networks (CNNs), have the potential to

improve shoreline classification accuracy by processing more robust remote sensing datasets and providing an end-to-end method that encompasses both segmentation and classification.

Refinement of the methodology used to quantify shoreline change would better align the rates with the erosion observed in the field following Hurricane Florence. Splitting the modified shoreline class into vertical and sloped sub-classes would provide additional context to how shoreline erosion rates are impacted by the modified structure in place. Added field sampling to obtain statistically significant sample sizes of these two sub-classes is recommended. Furthermore, change rate quantification in the NRE may improve through separate examination of the north and south shores as storm paths can change the wind and wave energy channeled into the estuary.

Additional applications to future shoreline management should also be explored beyond this study. The object-based ensemble analysis can be used to assess shoreline classification changes over time by using objects from a base year and substituting remotely sensed data from a different year to create new shoreline classification predictions. Observing how shoreline classifications evolve over time would provide coastal managers with valuable information that can be used to track both natural and engineered shoreline developments. It also has the potential to improve assessments of vulnerability by knowing how land cover has shifted over time.

The vulnerability assessment conducted within this study is highly adaptable and could also inform setback regulations within the NRE. Shoreline classification, coastal slope, and shoreline change are all variables that can be used to quantify how the distance of structures to water varies along different areas of the NRE. This information can then be used to improve setback regulations and reduce future hazards.

CHAPTER 6: CONCLUSIONS

Shoreline classification maps enable coastal communities to better understand erosion risks associated with different shoreline environments and are a tool for monitoring both natural and engineered changes along the shoreline. These maps also aid decision-makers, such as coastal managers, mitigating erosional hazards. Before this study, a recent, high-resolution shoreline classification map of the NRE did not exist. An object-based ensemble analysis approach is known to produce high accuracy classification results but has yet to be used in an estuarine shoreline environment such as the NRE. Therefore, this approach was applied to create an updated shoreline classification map of the NRE, evaluate the effectiveness of the object-based ensemble approach in an estuarine shoreline environment, and account for the effects of uncertainty within the final shoreline classification.

This study demonstrates that an object-based ensemble approach is an effective way to map shoreline classifications in the NRE. The object-based ensemble produced an overall accuracy of 76.4% and outperformed the pixel-based approach by 6.3%. By addressing known sources of error and limitations, the approach has the potential to reach accuracy percentages above 90%, but additional exploration is needed. This approach is advantageous compared to pixel-based classification as the resulting objects can be used to investigate numerous shoreline management applications.

An application of shoreline change and vulnerability assessment was explored within this study and produced shoreline change rates comparable to past studies in the NRE. However, a different approach to measuring shoreline change should be considered in future studies to better address the complex morphodynamics present in the NRE. As storm-induced erosion continues to

pose a significant threat to the NRE, refinement of these applications as well as new applications of the object-based ensemble analysis should continue to be explored to improve future shoreline management and reduce hazards moving forward.

CHAPTER 7: REFERENCES

Abuodha, P. A., & Woodroffe, C. D. (2010). Assessing vulnerability to sea-level rise using a coastal sensitivity index: a case study from southeast Australia. *Journal of Coastal Conservation*, *14*(3), 189-205.

Antonarakis, A. S., Richards, K. S., & Brasington, J. (2008). Object-based land cover classification using airborne LiDAR. *Remote Sensing of Environment*, *112*(6), 2988-2998.

Balica, S. F., Wright, N. G., & Van der Meulen, F. (2012). A flood vulnerability index for coastal cities and its use in assessing climate change impacts. *Natural Hazards*, *64*(1), 73-105.

Belgiu, M. & Dragut, L. (2016). Random Forest in Remote Sensing: A Review of Applications and Future Directions. *ISPRS Journal of Photogrammetry and Remote Sensing,* 114, 24-31. https://doi.org/10.1016/j.isprsjprs.2016.01.011

Benz, U.C., Hofmann, P., Willhauck, G., Lingenfelder, I., Heynen, M., (2004). Multiresolution, object-oriented fuzzy analysis of remote sensing data for GIS-ready information. *ISPRS Journal of Photogrammetry and Remote Sensing*, 58, 239–258.

Blaschke, T. (2010). Object based image analysis for remote sensing. *ISPRS Journal of Photogrammetry and Remote Sensing,* 65(1), 2-6. https://doi.org/10.1016/j.isprsjprs.2009.06.004

Boruff, B. J., Emrich, C., & Cutter, S. L. (2005). Erosion hazard vulnerability of US coastal counties. *Journal of Coastal Research*, *21*(5), 932-942.

Brennan, R., & Webster, T. L. (2006). Object-oriented land cover classification of lidar-derived surfaces. *Canadian Journal of Remote Sensing*, *32*(2), 162-172.

Bukvic, A., Rohat, G., Apotsos, A., & de Sherbinin, A. (2020). A systematic review of coastal vulnerability mapping. *Sustainability*, *12*(7), 2822.

Chan, J. C-W. & Paelinckx, D. (2008). Evaluation of Random Forest and Adaboost tree-based ensemble classification and spectral band selection for ecotope mapping use airborne hyperspectral imagery. *Remote Sensing of Environment*, 112, 2999-3011.

Choung, Y. J., & Jo, M. H. (2017). Comparison between a Machine-Learning-Based Method and a Water-Index-Based Method for Shoreline Mapping Using a High-Resolution Satellite Image Acquired in Hwado Island, South Korea. *Journal of Sensors*. https://doi.org/10.1155/2017/8245204

Congalton, R. G., & Green, K. (2019). *Assessing the accuracy of remotely sensed data: principles and practices*. CRC press.

Cooper, H. M., Zhang, C., Davis, S. E., & Troxler, T. G. (2019). Object-based correction of LiDAR DEMs using RTK-GPS data and machine learning modeling in the coastal Everglades. *Environmental Modelling & Software*, *112*, 179-191.

Corbett, D.R., Walsh, J. P., Cowart, L., Riggs, S. R., Ames, D. V, & Culver, S. J. (2008). Shoreline change within the Albemarle-Pamlico Estuarine System, North Carolina. *Department of Geological Sciences Thomas Harriot College of Arts and Sciences & Institute for Coastal Science and Policy East Carolina University.*

Cowart, L., Reide Corbett, D., & Walsh, J. P. (2011). Shoreline change along sheltered coastlines: Insights from the neuse river estuary, NC, USA. *Remote Sensing*, *3*(7), 1516–1534. https://doi.org/10.3390/rs3071516

Cowart, L.C., Walsh, J.P., & Corbett, D.R. (2010). Analyzing estuarine shoreline change: A case study of Cedar Island, NC. *J. Coast. Res*., 26, 817-830.

Crawford M.M., Ham J., Chen Y., & Ghosh J. (2003). Random forests of binary hierarchical classifiers for analysis of hyperspectral data. *IEEE Workshop on Advances in Techniques for Analysis of Remotely Sensed Data 27–28 Oct. 2003*, 337-345.

Crossett, K.M., Culliton, T.J., Wiley, P.C., & Goodspeed, T.R. (2004). *Population Trends along the Coastal United States: 1980–2008*. **http://www.oceanservice.noaa.gov/programs/mb/pdfs/coastal_pop_trends_complete.pdf.**

Dalponte, M., Orka, H.O., Gobakken, T., Gianelle, D., & Naesset, E. (2013). Tree species classification in boreal forests with hyperspectral data. *IEEE Transactions on Geoscience and Remote Sensing,* 51, 2632–2645.

Day Jr, J. W., Kemp, W. M., Yáñez-Arancibia, A., & Crump, B. C. (Eds.). (2012). *Estuarine Ecology*. John Wiley & Sons.

Demers, A., Banks, S., Pasher, J., Duffe, J., & Laforest, S. (2015). A comparative analysis of object-based and pixel-based classification of RADARSAT-2 C-band and optical satellite data for mapping shoreline types in the Canadian artic. *Canadian Journal of Remote Sensing*, 41(1), 1-19.

Diez, P. G., Perillo, G. M., & Piccolo, M. C. (2007). Vulnerability to sea-level rise on the coast of the Buenos Aires Province. *Journal of Coastal Research*, *23*(1), 119-126.

Doukakis, E. (2005). Coastal vulnerability and risk parameters. *European Water*, *11*(12), 3-7.

Du, P., Xia, J., Zhang, W., Tan, K., Liu, Y., & Liu, S. (2012). Multiple Classifier System for Remote Sensing Image Classification: A Review. *Sensors, 12*, 4764-4792.

Eulie, D. O., Walsh, J. P., Corbett, D. R., & Mulligan, R. P. (2017). Temporal and spatial dynamics of estuarine shoreline change in the Albemarle-Pamlico Estuarine System, North Carolina, USA. *Estuaries and Coasts*, *40*(3), 741-757.

Fan, R.-E., Chang, K.-W., Hsieh, C.-J., Wang, X.-R., & Lin. C.-J. (2008). LIBLINEAR: A Library for Large Linear Classification. *Journal of Machine Learning Research*, 9, 1871-1874.

Flood, M. (2001). Laser altimetry: From science to commercial lidar mapping. *Photogrammetric engineering and remote sensing*, *67*(11).

Frank, E., Hall, M.A., & Witten, I.H. (2016). *Data mining: Practical machine learning tools and techniques* (4th ed.). Cambridge, MA: Morgan Kaufmann.

Foody, G. M. (2004). Thematic map comparison. *Photogrammetric Engineering & Remote Sensing*, *70*(5), 627-633.

Foody, G. M., Boyd, D. S., & Sanchez-Hernandez, C. (2007). Mapping a specific class with an ensemble of classifiers. *International Journal of Remote Sensing*, *28*(8), 1733–1746. https://doi.org/10.1080/01431160600962566

Gerçek, D., Toprak, V., & Strobl, J. (2011). Object-based classification of landforms based on their local geometry and geomorphometric context. *International Journal of Geographical Information Science*, *25*(6), 1011-1023.

Gislason P.O., Benediktsson J.A., & Sveinsson J.R. (2006). Random Forests for land cover classification. *Pattern Recognition Letters*, 27, pp. 294-300.

Gornitz, V. (1990). Vulnerability of the East Coast, USA to future sea level rise. *Journal of Coastal Research*, 201-237.

Gornitz, V. M., Daniels, R. C., White, T. W., & Birdwell, K. R. (1994). The development of a coastal risk assessment database: vulnerability to sea-level rise in the US Southeast. *Journal of coastal research*, 327-338.

Hall, M., Frank, E., Holmes, G., Pfahringer, B., Reutemann, P., & Witten, I. (2009). The WEKA data mining software: An update. *SIGKDD Explorations, 11*, 10-18.

Ham J., Chen Y., Crawford M.M., & Ghosh J. (2005). Investigation of the Random Forest framework for classification of hyperspectral data. *IEEE Transactions on Geoscience and Remote Sensing*, 43, 492-501.

Hardaway Jr, C. S., & Gunn, J. R. (2010). Design and performance of headland bays in Chesapeake Bay, USA. *Coastal Engineering*, *57*(2), 203-212.

Hofmann, P., Blaschke, T., & Strobl, J. (2011). Quantifying the robustness of fuzzy rule sets in object-based image analysis. *International Journal of Remote Sensing*, *32*(22), 7359-7381.

Juel, A., Groom, G. B., Svenning, J. C., & Ejrnaes, R. (2015). Spatial application of Random Forest models for fine-scale coastal vegetation classification using object based analysis of aerial orthophoto and DEM data. *International Journal of Applied Earth Observation and Geoinformation*, *42*, 106-114.

Kaasalainen, S., Ahokas, E., Hyyppa, J., & Suomalainen, J. (2005). Study of surface brightness from backscattered laser intensity: Calibration of laser data. *IEEE Geoscience and Remote Sensing Letters*, *2*(3), 255-259.

Kampouraki, M., Wood, G. A., & Brewer, T. R. (2008). Opportunities and limitations of object based image analysis for detecting urban impervious and vegetated surfaces using true-colour aerial photography. In *Object-Based Image Analysis* (pp. 555-569). Springer, Berlin, Heidelberg.

Kantamaneni, K., Phillips, M., Thomas, T., & Jenkins, R. (2018). Assessing coastal vulnerability: Development of a combined physical and economic index. *Ocean & Coastal Management*, *158*, 164-175.

Koroglu, A., Ranasinghe, R., Jiménez, J. A., & Dastgheib, A. (2019). Comparison of coastal vulnerability index applications for Barcelona Province. *Ocean & coastal management*, *178*, 104799.

Kotaridis, I., & Lazaridou, M. (2021). Remote sensing image segmentation advances: A meta-analysis. *ISPRS Journal of Photogrammetry and Remote Sensing*, *173*, 309-322.

Kuncheva, L.I. (2004). Combining Pattern Classifiers: Methods and Algorithms; Wiley-Interscience: Hoboken, NJ, USA.

Landis, J. R., & Koch, G. G. (1977). The measurement of observer agreement for categorical data. *Biometrics*, 159-174.

Lawrence, R. L., Wood, S. D., & Sheley, R. L. (2006). Mapping invasive plants using hyperspectral imagery and Breiman Cutler classifications (RandomForest). *Remote Sensing of Environment*, *100*(3), 356-362.

Liu, D., & Xia, F. (2010). Assessing object-based classification: advantages and limitations. *Remote Sensing Letters*, *1*(4), 187-194.

Liu, W., Gopal, S., & Woodcock, C. E. (2004). Uncertainty and Confidence in Land Cover Classification Using a Hybrid Classifier Approach. http://cns-web.bu.edu

López Royo, M., Ranasinghe, R., & Jiménez, J. A. (2016). A rapid, low-cost approach to coastal vulnerability assessment at a national level. *Journal of Coastal Research*, *32*(4), 932-945.

Lorang, M. S., & Stanford, J. A. (1993). Variability of shoreline erosion and accretion within a beach compartment of Flathead Lake, Montana. *Limnology and oceanography*, *38*(8), 1783-1795.

Martha, T. R., Vamsee, A. M., Tripathi, V., & Kumar, K. V. (2018). Detection of coastal landforms in a deltaic area using a multi-scale object-based classification method. *Current Science*, *114*(6), 1338-1345.

Martin, D. M., Morton, T., Dobrzynski, T., & Valentine, B. (1996). Estuaries on the edge: The vital Link between land and sea.

Maxwell, A. E., Warner, T. A., & Fang, F. (2018). Implementation of machine-learning classification in remote sensing: An applied review. *International Journal of Remote Sensing*, *39*(9), 2784-2817.

Maxwell, A. E., Warner, T. A., Strager, M. P., Conley, J. F., & Sharp, A. L. (2015). Assessing machine-learning algorithms and image-and lidar-derived variables for GEOBIA classification of mining and mine reclamation. *International Journal of Remote Sensing*, *36*(4), 954-978.

McCarthy, M. J., & Halls, J. N. (2014). Habitat mapping and change assessment of coastal environments: an examination of WorldView-2, QuickBird, and IKONOS satellite imagery and airborne LiDAR for mapping barrier island habitats. *ISPRS International Journal of Geo-Information*, *3*(1), 297-325.

McCombs, J. W., Herold, N.D., Burkhalter, S.G. & Robinson, C.J. (2016). Accuracy Assessment of NOAA Coastal Change Analysis Program 2006-2010 Land Cover and Land Cover Change Data. *Photogrammetric Engineering & Remote Sensing*, 82(9), 711-718.

McVerry, K. (2012). *North Carolina Estuarine Shoreline Mapping Project Statewide and County Statistics*.

Mellor, A., Boukir, S., Haywood, A., & Jones, S. (2015). Exploring issues of training data imbalance and mislabelling on random forest performance for large area landcover classification using the ensemble margin. *ISPRS Journal of Photogrammetry and Remote Sensing,* 105, 155–168.

Millard, K. & Richardson, M. (2015). On the importance of training data sample selection in random forest image classification: a case study in peatland ecosystem mapping. *Remote Sensing,* 7, 8489.

Mohamad, M. F., Lee, L. H., & Samion, M. K. H. (2014). Coastal vulnerability assessment towards sustainable management of Peninsular Malaysia coastline. *International Journal of Environmental Science and Development*, *5*(6), 533.

Möller, M., Lymburner, L., & Volk, M. (2007). The comparison index: A tool for assessing the accuracy of image segmentation. *International Journal of Applied Earth Observation and Geoinformation*, *9*(3), 311-321.

Mountrakis, G., Im, J., & Ogole, C. (2011). Support vector machines in remote sensing: A review. *ISPRS Journal of Photogrammetry and Remote Sensing*, 66(3), 247–259.

Nageswara Rao, K., Subraelu, P., Venkateswara Rao, T., Hema Malini, B., Ratheesh, R., Bhattacharya, S., & Rajawat, A. S. (2008). Sea-level rise and coastal vulnerability: an assessment of Andhra Pradesh coast, India through remote sensing and GIS. *Journal of Coastal Conservation*, *12*(4), 195-207.

NC DEQ Division of Coastal Management. (2014). *CAMA Handbook for Coastal Development.* https://files.nc.gov/ncdeq/Coastal%20Management/documents/PDF/CAMA/CAMA%20Handbook%202014%20edition%20printable.pdf

Özyurt, G., & Ergin, A. (2010). Improving coastal vulnerability assessments to sea-level rise: a new indicator-based methodology for decision makers. *Journal of Coastal Research*, *26*(2), 265-273.

Paerl, H. W., Hall, N. S., Hounshell, A. G., Luettich, R. A., Rossignol, K. L., Osburn, C. L., & Bales, J. (2019). Recent increase in catastrophic tropical cyclone flooding in coastal North Carolina, USA: Long-term observations suggest a regime shift. *Scientific Reports*, *9*(1). https://doi.org/10.1038/s41598-019-46928-9

Palmer, B. J., Van der Elst, R., Mackay, F., Mather, A. A., Smith, A. M., Bundy, S. C., & Parak, O. (2011). Preliminary coastal vulnerability assessment for kwazulu-natal, south africa. *Journal of Coastal Research*, 1390-1395.

Pendleton, E. A., Williams, S. J., & Thieler, E. R. (2004). COASTAL VULNERABILITY ASSESSMENT OF ASSATEAGUE ISLAND NATIONAL SEASHORE (ASIS) TO SEA-LEVEL RISE. *US Geological Survey Open-File Report 2004-1020*. https://pubs.usgs.gov/of/2004/1020/html/cvi.htm

Phillips, J. (1999). Event Timing and Sequence in Coastal Shoreline Erosion: Hurricanes the Neuse Estuary. *Journal of Coastal Research*, 15(3).

Phillips, J. (2022). Geomorphic impacts of Hurricane Florence on the lower Neuse River: Portents and particulars. *Geomorphology*, 397, 108026

Polk, M. A., & Eulie, D. O. (2018). Effectiveness of Living Shorelines as an Erosion Control Method in North Carolina. *Estuaries and Coasts*, *41*(8), 2212–2222. https://doi.org/10.1007/s12237-018-0439-y

Qiu, F., & Jensen, J.R. (2004). Opening the black box of neural networks for remote sensing image classification. *International Journal of Remote Sensing*, 25(9), 1749-1768.

Riggs, S. R., & Ames, D. V. (2003). *DROWNING THE NORTH CAROLINA COAST:* Sea-Level Rise and Estuarine Dynamics. *North Carolina Sea Grant*.

Rogers, S., & Skrabal, T. E. (2001). The Soundfront Series: Managing Erosion on Estuarine Shorelines. *North Carolina Sea Grant.*

Ružić, I., Dugonjić Jovančević, S., Benac, Č., & Krvavica, N. (2019). Assessment of the Coastal Vulnerability Index in an area of complex geological conditions on the Krk Island, Northeast Adriatic Sea. *Geosciences*, *9*(5), 219.

Shaw, J., Taylor, R. B., Forbes, D. L., Ruz, M. H., & Solomon, S. (1998). *Sensitivity of the coasts of Canada to sea-level rise* (p. 114). Ottawa: Geological Survey of Canada.

Stewart, S. R., & Berg, R. (2019). National Hurricane Center Tropical Cyclone Report Hurricane Florence. https://www.nhc.noaa.gov/data/tcr/AL062018_Florence.pdf

Szuster, B. W., Chen, Q., & Borger, M. (2011). A comparison of classification techniques to support land cover and land use analysis in tropical coastal zones. *Applied Geography*, *31*(2), 525–532. https://doi.org/10.1016/j.apgeog.2010.11.007

Tonbul, H., Colkesen, I., & Kavzoglu, T. (2020). Classification of poplar trees with object-based ensemble learning algorithms using Sentinel-2A imagery. *Journal of Geodetic Science*, *10*(1), 14-22.

Thieler, E.R. and Hammer-Klose, E.S. 1999. National Assessment of Coastal Vulnerability to Sea-Level Rise, U.S. Atlantic Coast: U.S. Geological Survey Open-File Report 99-593.

Townshend, J. R. G., C. Huang, S. N. V. Kalluri, R. S. DeFries, S. Liang, and K. Yang. 2000. "Beware of per-Pixel Characterization of Land Cover." *International Journal of Remote Sensing* 21 (4): 839–843.

Trimble (2018). Trimble eCognition Developer for Windows Operating System 9.3.1 User Guide. Trimble. https://usermanual.wiki/Document/UserGuide.995437221.pdf

U.S. Geological Survey (2020). Surface Water data for North Carolina: USGS Surface-Water Annual Statistics. https://waterdata.usgs.gov/nc/nwis/annual?

Vali, A., Comai, S., & Matteucci, M. (2020). Deep learning for land use and land cover classification based on hyperspectral and multispectral earth observation data: A review. *Remote Sensing*, *12*(15), 2495.

Wang, X., Gao, X., Zhang, Y., Fei, X., Chen, Z., Wang, J., Zhang, Y., Lu, X., & Zhao, H. (2019). Land-cover classification of coastal wetlands using the RF algorithm for Worldview-2 and Landsat 8 images. *Remote Sensing*, *11*(16). https://doi.org/10.3390/rs11161927

Waske, B., Benediktsson, J. A., & Sveinsson, J. R. (2009). Classifying remote sensing data with support vector machines and imbalanced training data. In *International Workshop on Multiple Classifier Systems*, 375-384. Springer, Berlin, Heidelberg.

Wisner, B., Blaikie, P., Cannon, T., & Davis, I. (2014). At risk: natural hazards, people's vulnerability and disasters. Routledge.

Zhang, C. (2014). Combining hyperspectral and LiDAR data for vegetation mapping in the Florida Everglades. *ISPRS Journal of Photogrammetry and Remote Sensing, 80*, 733–743.

Zhang, C. (2015). Applying data fusion techniques for benthic habitat mapping and monitoring in a coral reef ecosystem. *ISPRS Journal of Photogrammetry and Remote Sensing, 104*, 213–223.

Zhang, C., Denka, S., Cooper, H., & Mishra, D. R. (2018). Quantification of sawgrass marsh aboveground biomass in the coastal Everglades using object-based ensemble analysis and Landsat data. *Remote Sensing of Environment*, *204*, 366–379. https://doi.org/10.1016/j.rse.2017.10.018

Zhang, C., Selch, D., & Cooper, H. (2016). A Framework to Combine Three Remotely Sensed Data Sources for Vegetation Mapping in the Central Florida Everglades. *Wetlands*, *36*(2), 201–213. https://doi.org/10.1007/s13157-015-0730-7

Zhang, C., Xie, Z., & Selch, D. (2013). Fusing lidar and digital aerial photography for object-based forest mapping in the Florida Everglades. *GIScience and Remote Sensing*, *50*(5), 562–573. https://doi.org/10.1080/15481603.2013.836807

Zhang, C., & Xie, Z. (2014). Data Fusion and Classifier Ensemble Techniques for Vegetation Mapping in the Coastal Everglades. *Geocarto International*, 29, 228-243.

Zhang, X., Han, L., Han, L., & Zhu, L. (2020). How well do deep learning-based methods for land cover classification and object detection perform on high resolution remote sensing imagery?. *Remote Sensing*, *12*(3), 417.

APPENDIX A: MACHINE LEARNING PARAMETER LOGS

1. Random Forest (RF)

RANDOM FOREST (RF)

		Attributes (Predictors)																											ML Parameters			
Date Run:	File Name	Brightness	Max Diff	R Mean	R Stdev	G Mean	G Stdev	B Mean	B Stdev	NIR Mean	NIR Stdev	Inten Mean	Inten Stdev	Lidar Mean	Lidar Med	Lidar Max	Lidar Min	Lidar Stdev	Lidar Mode	Slope Mean	Slope Med	Slope Max	Slope Min	Slope Stdev	NDVI Mean	NDVI Med	NDVI Max	NDVI Min	NDVI Stdev	Batch Size	num Iterations	Max Tree Depth	Accuracy (%)
7/21/21	Scale25 (now deleted)	x	x	x	x	x	x	x	x	x	x	x	x	x	x	x	x	x	x											100	100	unlimited	64.00%
7/28/21	ML_FieldDataset_PreQA	x	x	x	x	x	x	x	x	x	x	x	x	x	x	x	x	x	x											100	100	unlimited	66.00%
7/28/21	ML_FieldDataset_QA	x	x	x	x	x	x	x	x	x	x	x	x	x	x	x	x	x	x											100	100	unlimited	70.50%
7/28/21	ML_FieldDataset_QA	x	x	x	x	x	x	x	x	x	x	x	x	x	x	x	x	x	x											100	150	unlimited	70.33%
7/28/21	ML_FieldDataset_QA	x	x	x	x	x	x	x	x	x	x	x	x	x	x	x	x	x	x											100	200	unlimited	71.35%
7/28/21	ML_FieldDataset_QA	x	x	x	x	x	x	x	x	x	x	x	x	x	x	x	x	x	x											200	200	unlimited	71.35%
7/28/21	ML_FieldDataset_QA	x	x	x	x	x	x	x	x	x	x	x	x	x	x	x	x	x	x											200	100	unlimited	70.58%
7/28/21	ML_FieldDataset_QA	x	x	x	x	x	x	x	x	x	x	x	x	x	x	x	x	x	x											100	250	unlimited	70.84%
7/28/21	ML_FieldDataset_QA	x	x	x	x	x	x	x	x	x	x	x	x	x	x	x	x	x	x											100	300	unlimited	70.84%
7/28/21	ML_FieldDataset_QA	x	x	x	x	x	x	x	x	x	x	x	x	x	x	x	x	x	x											100	200	4	70.33%
7/28/21	ML_FieldDataset_QA	x	x	x	x	x	x	x	x	x	x	x	x	x	x	x	x	x	x											100	200	5	71.61%
7/28/21	ML_FieldDataset_QA	x	x	x	x	x	x	x	x	x	x	x	x	x	x	x	x	x	x											100	200	6	70.32%
7/28/21	ML_FieldDataset_QA	x	x	x	x	x	x	x	x	x	x	x	x	x	x	x	x	x	x											100	300	5	71.61%
7/28/21	ML_FieldDataset_QA	x	x	x	x	x	x	x	x	x	x	x	x	x	x	x	x	x	x											100	250	5	71.35%
7/28/21	ML_FieldDataset_QA	x	x	x	x	x	x	x	x	x	x	x	x	x	x	x	x	x	x											100	150	5	71.87%
7/28/21	ML_FieldDataset_QA	x	x	x	x	x	x	x	x	x	x	x	x	x	x	x	x	x	x											100	100	5	71.25%
9/17/21	ML_Dataset_QA_NewPredicts	x	x	x	x	x	x	x	x	x	x	x	x	x	x	x	x	x	x	x	x	x	x	x	x	x	x	x	x	100	150	5	73.01%
9/17/21	ML_Dataset_QA_NewPredicts	x	x	x	x	x	x	x	x	x	x	x	x	x	x	x	x	x	x	x	x	x	x	x	x	x	x	x	x	100	250	unlimited	72.49%
9/17/21	ML_Dataset_QA_NewPredicts	x	x	x	x	x	x	x	x	x	x	x	x	x	x	x	x	x	x	x	x	x	x	x	x	x	x	x	x	100	200	5	72.75%
9/17/21	ML_Dataset_QA_NewPredicts	x	x	x	x	x	x	x	x	x	x	x	x	x	x	x	x	x	x	x	x	x	x	x	x	x	x	x	x	100	250	5	72.49%
9/27/21	ML_Dataset_QA_NewPredicts			x	x	x	x	x	x	x	x	x	x	x	x	x	x	x	x	x	x	x	x	x	x	x	x	x	x	100	150	5	70.95%
9/27/21	ML_Dataset_QA_NewPredicts	x	x			x	x	x	x	x	x	x	x	x	x	x	x	x	x	x	x	x	x	x	x	x	x	x	x	100	150	5	72.49%
9/27/21	ML_Dataset_QA_NewPredicts	x	x	x	x			x	x	x	x	x	x	x	x	x	x	x	x	x	x	x	x	x	x	x	x	x	x	100	150	5	73.52%
9/27/21	ML_Dataset_QA_NewPredicts	x	x	x	x	x	x			x	x	x	x	x	x	x	x	x	x	x	x	x	x	x	x	x	x	x	x	100	150	5	72.24%
9/27/21	ML_Dataset_QA_NewPredicts	x	x	x	x	x	x	x	x			x	x	x	x	x	x	x	x	x	x	x	x	x	x	x	x	x	x	100	150	5	73.01%
9/27/21	ML_Dataset_QA_NewPredicts	x	x	x	x	x	x	x	x	x	x			x	x	x	x	x	x	x	x	x	x	x	x	x	x	x	x	100	150	5	72.49%
9/27/21	ML_Dataset_QA_NewPredicts	x	x	x	x			x	x			x	x	x	x	x	x	x	x	x	x	x	x	x	x	x	x	x	x	100	150	5	72.49%
9/27/21	ML_Dataset_QA_NewPredicts	x	x	x	x			x	x	x	x	x	x	x	x	x	x	x	x	x	x	x	x	x						100	150	5	71.47%
9/27/21	ML_Dataset_QA_NewPredicts	x	x	x	x			x	x	x	x	x	x	x	x	x	x	x	x	x	x	x	x	x						100	150	5	71.21%
9/27/21	ML_Dataset_QA_NewPredicts	x	x	x	x			x	x	x	x	x	x	x	x	x	x	x	x						x	x	x	x	x	100	150	5	72.75%
9/27/21	ML_Dataset_QA_NewPredicts	x	x	x	x			x	x	x	x	x	x							x	x	x	x	x	x	x	x	x	x	100	150	5	67.61%
9/27/21	ML_Dataset_QA_NewPredicts	x	x							x		x		x	x	x	x								x					100	150	5	72.24%
9/27/21	ML_Dataset_QA_NewPredicts	x	x	x				x		x		x								x					x					100	150	5	69.92%
9/27/21	ML_Dataset_QA_NewPredicts	x	x	x				x		x		x										x	x				x	x		100	150	5	73.52%
9/27/21	ML_Dataset_QA_NewPredicts	x	x	x				x		x		x				x	x					x	x		x		x	x		100	150	5	74.29%
9/27/21	ML_Dataset_QA_NewPredicts	x	x	x						x		x				x	x			x		x	x				x	x		100	150	5	72.49%

2. k-Nearest Neighbor (kNN)

k-Nearest Neighbor (kNN)

		Attributes (Predictors)																												ML Parameters					
Date Run:	File Name	Brightness	Max Diff	R Mean	R Stdev	G Mean	G Stdev	B Mean	B Stdev	NIR Mean	NIR Stdev	Inten Mean	Inten Stdev	Lidar Mean	Lidar Med	Lidar Max	Lidar Min	Lidar Stdev	Lidar Mode	Slope Mean	Slope Med	Slope Max	Slope Min	Slope Stdev	NDVI Mean	NDVI Med	NDVI Max	NDVI Min	NDVI Stdev	k	Batch Size	Distance Weighting	Search Algorithm	Distance Function	Accuracy (%)
7/21/21	Scale25 (now deleted)	x	x	x	x	x	x	x	x	x	x	x	x	x	x	x	x	x	x											3	100	N	LinearNNSearch	EuclideanDistance	57.00%
7/28/21	ML_FieldDataset_PreQA	x	x	x	x	x	x	x	x	x	x	x	x	x	x	x	x	x	x											3	100	N	LinearNNSearch	EuclideanDistance	58.00%
7/28/21	ML_FieldDataset_QA	x	x	x	x	x	x	x	x	x	x	x	x	x	x	x	x	x	x											3	100	N	LinearNNSearch	EuclideanDistance	61.00%
7/28/21	ML_FieldDataset_QA	x	x	x	x	x	x	x	x	x	x	x	x	x	x	x	x	x	x											3	150	N	LinearNNSearch	EuclideanDistance	61.64%
7/28/21	ML_FieldDataset_QA	x	x	x	x	x	x	x	x	x	x	x	x	x	x	x	x	x	x											3	200	N	LinearNNSearch	EuclideanDistance	61.64%
7/28/21	ML_FieldDataset_QA	x	x	x	x	x	x	x	x	x	x	x	x	x	x	x	x	x	x											3	300	N	LinearNNSearch	EuclideanDistance	61.64%
7/28/21	ML_FieldDataset_QA	x	x	x	x	x	x	x	x	x	x	x	x	x	x	x	x	x	x											3	150	1/distance	LinearNNSearch	EuclideanDistance	62.92%
7/28/21	ML_FieldDataset_QA	x	x	x	x	x	x	x	x	x	x	x	x	x	x	x	x	x	x											3	200	1/distance	LinearNNSearch	EuclideanDistance	62.92%
7/28/21	ML_FieldDataset_QA	x	x	x	x	x	x	x	x	x	x	x	x	x	x	x	x	x	x											3	100	1/distance	LinearNNSearch	EuclideanDistance	62.92%
7/28/21	ML_FieldDataset_QA	x	x	x	x	x	x	x	x	x	x	x	x	x	x	x	x	x	x											3	150	1 - distance	LinearNNSearch	EuclideanDistance	62.66%
7/28/21	ML_FieldDataset_QA	x	x	x	x	x	x	x	x	x	x	x	x	x	x	x	x	x	x											3	200	1 - distance	LinearNNSearch	EuclideanDistance	62.66%
8/2/21	ML_FieldDataset_QA	x	x	x	x	x	x	x	x	x	x	x	x	x	x	x	x	x	x											3	200	1/distance	LinearNNSearch	ChebyshevDistance	58.31%
8/2/21	ML_FieldDataset_QA	x	x	x	x	x	x	x	x	x	x	x	x	x	x	x	x	x	x											3	200	1/distance	LinearNNSearch	FilteredDistance	54.48%
8/2/21	ML_FieldDataset_QA	x	x	x	x	x	x	x	x	x	x	x	x	x	x	x	x	x	x											3	200	1/distance	LinearNNSearch	ManhattanDistance	63.17%
8/2/21	ML_FieldDataset_QA	x	x	x	x	x	x	x	x	x	x	x	x	x	x	x	x	x	x											3	200	1/distance	LinearNNSearch	MinkowskiDistance	62.92%
8/2/21	ML_FieldDataset_QA	x	x	x	x	x	x	x	x	x	x	x	x	x	x	x	x	x	x											3	200	N	LinearNNSearch	ManhattanDistance	64.19%
8/2/21	ML_FieldDataset_QA	x	x	x	x	x	x	x	x	x	x	x	x	x	x	x	x	x	x											3	200	1 - distance	LinearNNSearch	ManhattanDistance	63.17%
8/2/21	ML_FieldDataset_QA	x	x	x	x	x	x	x	x	x	x	x	x	x	x	x	x	x	x											3	200	N	BallTree	EuclideanDistance	61.63%
8/2/21	ML_FieldDataset_QA	x	x	x	x	x	x	x	x	x	x	x	x	x	x	x	x	x	x											3	200	1 - distance	BallTree	EuclideanDistance	62.66%
8/2/21	ML_FieldDataset_QA	x	x	x	x	x	x	x	x	x	x	x	x	x	x	x	x	x	x											3	200	1/distance	BallTree	EuclideanDistance	62.91%
8/2/21	ML_FieldDataset_QA	x	x	x	x	x	x	x	x	x	x	x	x	x	x	x	x	x	x											3	200	N	CoverTree	EuclideanDistance	61.64%
8/2/21	ML_FieldDataset_QA	x	x	x	x	x	x	x	x	x	x	x	x	x	x	x	x	x	x											3	200	1 - distance	CoverTree	EuclideanDistance	62.66%
8/2/21	ML_FieldDataset_QA	x	x	x	x	x	x	x	x	x	x	x	x	x	x	x	x	x	x											3	200	1/distance	CoverTree	EuclideanDistance	62.92%
8/2/21	ML_FieldDataset_QA	x	x	x	x	x	x	x	x	x	x	x	x	x	x	x	x	x	x											3	200	N	FilteredNeighborhoodSearch	EuclideanDistance	61.64%
8/2/21	ML_FieldDataset_QA	x	x	x	x	x	x	x	x	x	x	x	x	x	x	x	x	x	x											3	200	1/distance	FilteredNeighborhoodSearch	EuclideanDistance	62.92%
8/2/21	ML_FieldDataset_QA	x	x	x	x	x	x	x	x	x	x	x	x	x	x	x	x	x	x											3	200	1 - distance	FilteredNeighborhoodSearch	EuclideanDistance	62.66%
8/2/21	ML_FieldDataset_QA	x	x	x	x	x	x	x	x	x	x	x	x	x	x	x	x	x	x											3	200	N	KDTree	EuclideanDistance	61.63%
8/2/21	ML_FieldDataset_QA	x	x	x	x	x	x	x	x	x	x	x	x	x	x	x	x	x	x											3	200	1/distance	KDTree	EuclideanDistance	62.92%
8/2/21	ML_FieldDataset_QA	x	x	x	x	x	x	x	x	x	x	x	x	x	x	x	x	x	x											3	200	1 - distance	KDTree	EuclideanDistance	62.66%
9/17/21	ML_Dataset_QA_NewPredicts	x	x	x	x	x	x	x	x	x	x	x	x	x	x	x	x	x	x	x	x	x	x	x	x	x	x	x	x	3	200	N	LinearNNSearch	ManhattanDistance	67.35%
9/17/21	ML_Dataset_QA_NewPredicts	x	x	x	x	x	x	x	x	x	x	x	x	x	x	x	x	x	x	x	x	x	x	x	x	x	x	x	x	3	150	N	LinearNNSearch	ManhattanDistance	67.35%
9/17/21	ML_Dataset_QA_NewPredicts	x	x	x	x	x	x	x	x	x	x	x	x	x	x	x	x	x	x	x	x	x	x	x	x	x	x	x	x	3	250	N	LinearNNSearch	ManhattanDistance	67.35%
9/17/21	ML_Dataset_QA_NewPredicts	x	x	x	x	x	x	x	x	x	x	x	x	x	x	x	x	x	x	x	x	x	x	x	x	x	x	x	x	3	200	1/distance	LinearNNSearch	ManhattanDistance	67.10%
9/17/21	ML_Dataset_QA_NewPredicts	x	x	x	x	x	x	x	x	x	x	x	x	x	x	x	x	x	x	x	x	x	x	x	x	x	x	x	x	3	200	1 - distance	LinearNNSearch	ManhattanDistance	67.10%
9/17/21	ML_Dataset_QA_NewPredicts	x	x	x	x	x	x	x	x	x	x	x	x	x	x	x	x	x	x	x	x	x	x	x	x	x	x	x	x	3	200	N	FilteredNeighborhoodSearch	ManhattanDistance	64.78%
9/17/21	ML_Dataset_QA_NewPredicts	x	x	x	x	x	x	x	x	x	x	x	x	x	x	x	x	x	x	x	x	x	x	x	x	x	x	x	x	3	200	1/distance	FilteredNeighborhoodSearch	EuclideanDistance	63.75%
9/17/21	ML_Dataset_QA_NewPredicts	x	x	x	x	x	x	x	x	x	x	x	x	x	x	x	x	x	x	x	x	x	x	x	x	x	x	x	x	3	200	1 - distance	FilteredNeighborhoodSearch	EuclideanDistance	63.75%
9/17/21	ML_Dataset_QA_NewPredicts	x	x	x	x	x	x	x	x	x	x	x	x	x	x	x	x	x	x	x	x	x	x	x	x	x	x	x	x	3	200	N	BallTree	EuclideanDistance	64.78%
9/17/21	ML_Dataset_QA_NewPredicts	x	x	x	x	x	x	x	x	x	x	x	x	x	x	x	x	x	x	x	x	x	x	x	x	x	x	x	x	3	200	1/distance	BallTree	EuclideanDistance	63.75%
9/17/21	ML_Dataset_QA_NewPredicts	x	x	x	x	x	x	x	x	x	x	x	x	x	x	x	x	x	x	x	x	x	x	x	x	x	x	x	x	3	200	1 - distance	BallTree	EuclideanDistance	63.75%
9/17/21	ML_Dataset_QA_NewPredicts	x	x	x	x	x	x	x	x	x	x	x	x	x	x	x	x	x	x	x	x	x	x	x	x	x	x	x	x	3	200	N	KDTree	EuclideanDistance	64.78%
9/17/21	ML_Dataset_QA_NewPredicts	x	x	x	x	x	x	x	x	x	x	x	x	x	x	x	x	x	x	x	x	x	x	x	x	x	x	x	x	3	200	N	CoverTree	EuclideanDistance	64.78%
9/27/21	ML_Dataset_QA_NewPredicts			x	x	x	x	x	x	x	x	x	x	x	x	x	x	x	x	x	x	x	x	x	x	x	x	x	x	3	200	N	LinearNNSearch	ManhattanDistance	69.15%
9/27/21	ML_Dataset_QA_NewPredicts	x	x			x	x	x	x	x	x	x	x	x	x	x	x	x	x	x	x	x	x	x	x	x	x	x	x	3	200	N	LinearNNSearch	ManhattanDistance	67.10%
9/27/21	ML_Dataset_QA_NewPredicts	x	x	x	x			x	x	x	x	x	x	x	x	x	x	x	x	x	x	x	x	x	x	x	x	x	x	3	200	N	LinearNNSearch	ManhattanDistance	67.61%
9/27/21	ML_Dataset_QA_NewPredicts	x	x	x	x	x	x			x	x	x	x	x	x	x	x	x	x	x	x	x	x	x	x	x	x	x	x	3	200	N	LinearNNSearch	ManhattanDistance	67.61%
9/27/21	ML_Dataset_QA_NewPredicts	x	x	x	x	x	x	x	x	x	x	x	x	x	x	x	x	x	x	x	x	x	x	x	x	x	x	x	x	3	200	N	LinearNNSearch	ManhattanDistance	67.61%
9/27/21	ML_Dataset_QA_NewPredicts	x	x	x	x	x	x	x	x	x	x	x	x	x	x	x	x	x	x	x	x	x	x	x	x	x	x	x	x	3	200	N	LinearNNSearch	ManhattanDistance	66.84%
9/27/21	ML_Dataset_QA_NewPredicts			x	x	x	x	x	x	x	x	x	x	x	x	x	x	x	x											3	200	N	LinearNNSearch	ManhattanDistance	64.78%
9/27/21	ML_Dataset_QA_NewPredicts			x	x	x	x	x	x	x	x	x	x	x	x	x	x	x	x	x	x	x	x	x						3	200	N	LinearNNSearch	ManhattanDistance	68.12%
9/27/21	ML_Dataset_QA_NewPredicts			x	x	x	x	x	x	x	x	x	x	x	x	x	x	x	x						x	x	x	x	x	3	200	N	LinearNNSearch	ManhattanDistance	63.49%
9/27/21	ML_Dataset_QA_NewPredicts			x	x	x	x	x	x	x	x	x	x	x	x	x	x	x	x	x	x	x	x	x	x		x	x		3	200	N	LinearNNSearch	ManhattanDistance	67.09%
9/27/21	ML_Dataset_QA_NewPredicts			x	x	x	x	x	x	x	x	x	x	x	x		x			x	x	x	x		x		x	x		3	200	N	LinearNNSearch	ManhattanDistance	65.04%
9/27/21	ML_Dataset_QA_NewPredicts			x	x	x	x	x	x	x	x	x	x	x	x	x	x	x	x	x	x	x	x	x	x					3	200	N	LinearNNSearch	ManhattanDistance	67.61%
9/27/21	ML_Dataset_QA_NewPredicts			x		x		x		x		x		x	x					x	x		x							3	200	N	LinearNNSearch	ManhattanDistance	64.27%

3. Support Vector Machine (SVM)

Support Vector Machine (SVM)

		Attributes (Predictors)																		ML Parameters					
Date Run:	File Name	Brightness	Max Diff	R Mean	R-Stdev	G Mean	G Stdev	B Mean	B Stdev	NIR Mean	NIR Stdev	Inten Mean	Inten Stdev	Lidar Mean	Lidar Med	Lidar Max	Lidar Min	Lidar Stdev	Lidar Mode	Batch Size	degree	Kernel Type	Shrinking Heuristic	eps	Accuracy (%)
7/21/21	Scale25 (now deleted)	x	x	x	x	x	x	x	x	x	x	x	x	x	x	x	x	x	x	100	3	linear	TRUE	0.001	63.00%
7/28/21	ML_FieldDataset_PreQA	x	x	x	x	x	x	x	x	x	x	x	x	x	x	x	x	x	x	100	3	linear	TRUE	0.001	65.00%
7/28/21	ML_FieldDataset_QA	x	x	x	x	x	x	x	x	x	x	x	x	x	x	x	x	x	x	100	3	linear	TRUE	0.001	69.05%
8/2/21	ML_FieldDataset_QA	x	x	x	x	x	x	x	x	x	x	x	x	x	x	x	x	x	x	200	3	linear	TRUE	0.001	69.05%
8/2/21	ML_FieldDataset_QA	x	x	x	x	x	x	x	x	x	x	x	x	x	x	x	x	x	x	100	3	linear	FALSE	0.001	69.31%
8/2/21	ML_FieldDataset_QA	x	x	x	x	x	x	x	x	x	x	x	x	x	x	x	x	x	x	100	3	radial basis function	TRUE	0.001	42.97%
8/2/21	ML_FieldDataset_QA	x	x	x	x	x	x	x	x	x	x	x	x	x	x	x	x	x	x	100	3	sigmoidal	TRUE	0.001	42.97%
8/2/21	ML_FieldDataset_QA	x	x	x	x	x	x	x	x	x	x	x	x	x	x	x	x	x	x	100	3	polynomial	TRUE	0.001	61.64%
8/2/21	ML_FieldDataset_QA	x	x	x	x	x	x	x	x	x	x	x	x	x	x	x	x	x	x	100	3	polynomial	FALSE	0.001	61.64%
9/17/21	ML_Dataset_QA_NewPredicts	x	x	x	x	x	x	x	x	x	x	x	x	x	x	x	x	x	x	100	3	linear	FALSE	0.001	70.18%
9/17/21	ML_Dataset_QA_NewPredicts	x	x	x	x	x	x	x	x	x	x	x	x	x	x	x	x	x	x	100	3	radial basis function	TRUE	0.001	43.19%
9/17/21	ML_Dataset_QA_NewPredicts	x	x	x	x	x	x	x	x	x	x	x	x	x	x	x	x	x	x	100	3	polynomial	TRUE	0.001	64.30%
9/17/21	ML_Dataset_QA_NewPredicts	x	x	x	x	x	x	x	x	x	x	x	x	x	x	x	x	x	x	100	3	sigmoidal	TRUE	0.001	43.19%
9/17/21	ML_Dataset_QA_NewPredicts	x	x	x	x	x	x	x	x	x	x	x	x	x	x	x	x	x	x	100	2	linear	TRUE	0.001	70.18%
9/17/21	ML_Dataset_QA_NewPredicts	x	x	x	x	x	x	x	x	x	x	x	x	x	x	x	x	x	x	100	2	linear	FALSE	0.001	70.18%
9/17/21	ML_Dataset_QA_NewPredicts	x	x	x	x	x	x	x	x	x	x	x	x	x	x	x	x	x	x	100	4	linear	FALSE	0.001	70.18%
9/17/21	ML_Dataset_QA_NewPredicts	x	x	x	x	x	x	x	x	x	x	x	x	x	x	x	x	x	x	100	3	linear	TRUE	0.001	70.18%
9/17/21	ML_Dataset_QA_NewPredicts	x	x	x	x	x	x	x	x	x	x	x	x	x	x	x	x	x	x	100	3	linear	FALSE	0.0001	70.18%
9/17/21	ML_Dataset_QA_NewPredicts	x	x	x	x	x	x	x	x	x	x	x	x	x	x	x	x	x	x	100	3	linear	FALSE	0.00001	70.18%
9/27/21	ML_Dataset_QA_NewPredicts			x	x	x	x	x	x	x	x	x	x	x	x	x	x	x	x	100	3	linear	FALSE	0.001	70.69%
9/27/21	ML_Dataset_QA_NewPredicts	x	x			x	x	x	x	x	x	x	x	x	x	x	x	x	x	100	3	linear	FALSE	0.001	68.38%
9/27/21	ML_Dataset_QA_NewPredicts	x	x	x	x			x	x	x	x	x	x	x	x	x	x	x	x	100	3	linear	FALSE	0.001	70.95%
9/27/21	ML_Dataset_QA_NewPredicts	x	x	x	x	x	x			x	x	x	x	x	x	x	x	x	x	100	3	linear	FALSE	0.001	68.38%
9/27/21	ML_Dataset_QA_NewPredicts	x	x	x	x	x	x	x	x			x	x	x	x	x	x	x	x	100	3	linear	FALSE	0.001	67.87%
9/27/21	ML_Dataset_QA_NewPredicts	x	x	x	x	x	x	x	x	x	x			x	x	x	x	x	x	100	3	linear	FALSE	0.001	70.69%
9/27/21	ML_Dataset_QA_NewPredicts				x	x			x	x	x			x	x	x	x	x	x	100	3	linear	FALSE	0.001	66.07%
9/27/21	ML_Dataset_QA_NewPredicts	x	x	x	x				x	x	x	x	x	x	x	x	x	x	x	100	3	linear	FALSE	0.001	69.92%
9/27/21	ML_Dataset_QA_NewPredicts	x	x	x	x				x	x	x	x	x	x	x	x	x	x	x	100	3	linear	FALSE	0.001	69.67%
9/27/21	ML_Dataset_QA_NewPredicts	x	x	x	x				x	x	x	x	x	x	x	x	x	x	x	100	3	linear	FALSE	0.001	70.43%
9/27/21	ML_Dataset_QA_NewPredicts	x	x	x	x				x	x	x	x	x							100	3	linear	FALSE	0.001	68.12%
9/27/21	ML_Dataset_QA_NewPredicts	x	x	x	x				x	x	x	x	x	x	x	x	x	x	x	100	3	linear	FALSE	0.001	69.29%
9/27/21	ML_Dataset_QA_NewPredicts	x	x	x	x				x	x	x	x	x	x	x	x	x	x	x	100	3	linear	FALSE	0.001	71.24%
9/27/21	ML_Dataset_QA_NewPredicts	x	x	x	x				x	x	x	x	x	x	x	x	x	x	x	100	3	linear	FALSE	0.001	71.72%
9/27/21	ML_Dataset_QA_NewPredicts	x	x	x	x				x	x	x	x	x	x	x	x	x	x	x	100	3	linear	FALSE	0.001	71.21%
9/27/21	ML_Dataset_QA_NewPredicts	x	x	x	x				x	x	x	x	x	x	x	x	x	x	x	100	3	linear	FALSE	0.001	71.47%
9/27/21	ML_Dataset_QA_NewPredicts	x	x	x	x				x	x	x	x	x	x	x	x	x	x	x	100	3	linear	FALSE	0.001	70.95%
9/27/21	ML_Dataset_QA_NewPredicts	x	x	x					x			x		x	x	x	x	x		100	3	linear	FALSE	0.001	72.24%

4. libLINEAR (LL)

libLINEAR

		Attributes (Predictors)																		ML Parameters					
Date Run:	File Name	Brightness	Max Diff	R Mean	R-Stdev	G Mean	G Stdev	B Mean	B Stdev	NIR Mean	NIR Stdev	Inten Mean	Inten Stdev	Lidar Mean	Lidar Med	Lidar Max	Lidar Min	Lidar Stdev	Lidar Mode	Batch Size	SVM Type	Bias	Max Num Iterations	cost (C)	Accuracy (%)
8/2/21	ML_FieldDataset_QA	x	x	x	x	x	x	x	x	x	x	x	x	x	x	x	x	x	x	100	L2-regularized L2-loss SVC (primal)	1	1000	1	70.08%
8/2/21	ML_FieldDataset_QA	x	x	x	x	x	x	x	x	x	x	x	x	x	x	x	x	x	x	200	L2-regularized L2-loss SVC (primal)	1	1000	1	70.08%
8/2/21	ML_FieldDataset_QA	x	x	x	x	x	x	x	x	x	x	x	x	x	x	x	x	x	x	100	L2-regularized L2-loss SVC (primal)	1	1000	2	70.84%
8/2/21	ML_FieldDataset_QA	x	x	x	x	x	x	x	x	x	x	x	x	x	x	x	x	x	x	100	L2-regularized L2-loss SVC (primal)	1	1000	3	70.58%
8/2/21	ML_FieldDataset_QA	x	x	x	x	x	x	x	x	x	x	x	x	x	x	x	x	x	x	100	L2-regularized L2-loss SVC (primal)	1	2000	2	70.84%
8/2/21	ML_FieldDataset_QA	x	x	x	x	x	x	x	x	x	x	x	x	x	x	x	x	x	x	100	L2-regularized L2-loss SVC (primal)	1	500	2	70.84%
8/2/21	ML_FieldDataset_QA	x	x	x	x	x	x	x	x	x	x	x	x	x	x	x	x	x	x	100	L2-regularized L2-loss SVC (primal)	0	1000	2	70.33%
8/2/21	ML_FieldDataset_QA	x	x	x	x	x	x	x	x	x	x	x	x	x	x	x	x	x	x	100	L2-regularized L2-loss SVC (primal)	2	1000	2	71.36%
8/2/21	ML_FieldDataset_QA	x	x	x	x	x	x	x	x	x	x	x	x	x	x	x	x	x	x	100	L2-regularized L2-loss SVC (primal)	3	1000	2	71.10%
8/2/21	ML_FieldDataset_QA	x	x	x	x	x	x	x	x	x	x	x	x	x	x	x	x	x	x	100	L2-regularized L2-loss SVC (primal)	1.5	1000	2	70.08%
9/17/21	ML_Dataset_QA_NewPredicts	x	x	x	x	x	x	x	x	x	x	x	x	x	x	x	x	x	x	100	L2-regularized L2-loss SVC (primal)	2	1000	2	70.43%
9/17/21	ML_Dataset_QA_NewPredicts	x	x	x	x	x	x	x	x	x	x	x	x	x	x	x	x	x	x	100	L2-regularized L2-loss SVC (primal)	1	1000	2	71.72%
9/17/21	ML_Dataset_QA_NewPredicts	x	x	x	x	x	x	x	x	x	x	x	x	x	x	x	x	x	x	100	L2-regularized L2-loss SVC (primal)	2	1000	3	71.21%
9/27/21	ML_Dataset_QA_NewPredicts			x	x	x	x	x	x	x	x	x	x	x	x	x	x	x	x	100	L2-regularized L2-loss SVC (primal)	1	1000	2	71.21%
9/27/21	ML_Dataset_QA_NewPredicts	x	x			x	x	x	x	x	x	x	x	x	x	x	x	x	x	100	L2-regularized L2-loss SVC (primal)	1	1000	2	66.07%
9/27/21	ML_Dataset_QA_NewPredicts	x	x	x	x			x	x	x	x	x	x	x	x	x	x	x	x	100	L2-regularized L2-loss SVC (primal)	1	1000	2	69.41%
9/27/21	ML_Dataset_QA_NewPredicts	x	x	x	x	x	x			x	x	x	x	x	x	x	x	x	x	100	L2-regularized L2-loss SVC (primal)	1	1000	2	69.92%
9/27/21	ML_Dataset_QA_NewPredicts	x	x	x	x	x	x	x	x			x	x	x	x	x	x	x	x	100	L2-regularized L2-loss SVC (primal)	1	1000	2	69.92%
9/27/21	ML_Dataset_QA_NewPredicts	x	x	x	x	x	x	x	x	x	x			x	x	x	x	x	x	100	L2-regularized L2-loss SVC (primal)	1	1000	2	70.18%
9/27/21	ML_Dataset_QA_NewPredicts	x	x	x	x	x	x	x	x	x	x	x	x	x	x	x	x	x	x	100	L2-regularized L2-loss SVC (primal)	1	1000	2	72.75%
9/27/21	ML_Dataset_QA_NewPredicts	x	x	x	x	x	x	x	x	x	x	x	x	x	x	x	x	x	x	100	L2-regularized L2-loss SVC (primal)	1	1000	2	69.92%
9/27/21	ML_Dataset_QA_NewPredicts	x	x	x	x	x	x	x	x	x	x	x	x	x	x	x	x	x	x	100	L2-regularized L2-loss SVC (primal)	1	1000	2	71.98%
9/27/21	ML_Dataset_QA_NewPredicts	x	x	x	x	x	x	x	x	x	x	x	x	x	x	x	x	x	x	100	L2-regularized L2-loss SVC (primal)	1	1000	2	69.92%
9/27/21	ML_Dataset_QA_NewPredicts	x	x	x	x	x	x	x	x	x	x	x	x	x	x	x	x	x	x	100	L2-regularized L2-loss SVC (primal)	1	1000	2	73.78%
9/27/21	ML_Dataset_QA_NewPredicts	x	x	x	x	x	x	x	x	x	x	x	x	x	x	x	x	x	x	100	L2-regularized L2-loss SVC (primal)	1	1000	2	72.75%
9/27/21	ML_Dataset_QA_NewPredicts	x		x	x	x	x	x	x	x	x	x	x	x	x	x	x	x		100	L2-regularized L2-loss SVC (primal)	1	1000	2	74.04%
9/27/21	ML_Dataset_QA_NewPredicts	x		x		x		x		x		x	x	x	x	x	x	x		100	L2-regularized L2-loss SVC (primal)	1	1000	2	69.92%
9/27/21	ML_Dataset_QA_NewPredicts	x		x	x	x	x	x	x	x	x	x	x	x	x	x	x	x		100	L2-regularized L2-loss SVC (primal)	2	100	2	74.29%

5. Artificial Neural Network (ANN)

Multilayer Perceptron (ANN)

		Attributes (Predictors)																										ML Parameters					
Date Run:	File Name	Brightness	Max Diff	R Mean	R Stdev	G Mean	G Stdev	B Mean	B Stdev	NIR Mean	NIR Stdev	Inten Mean	Inten Stdev	Lidar Mean	Lidar Med	Lidar Max	Lidar Min	Lidar Stdev	Lidar Mode	Slope Mean	Slope Med	Slope Max	Slope Min	Slope Stdev	NDVI Mean	NDVI Med	NDVI Max	NDVI Min	NDVI Stdev	Batch Size	Hidden Layers	Learning Rate	momentum	Training Time	Accuracy (%)
9/17/21	ML_Dataset_QA_NewPredicts	x	x	x	x	x	x	x	x	x	x	x	x	x	x	x	x	x	x	x	x	x	x	x	x	x	x	x	x	100	a	0.3	0.2	500	70.18%
9/17/21	ML_Dataset_QA_NewPredicts	x	x	x	x	x	x	x	x	x	x	x	x	x	x	x	x	x	x	x	x	x	x	x	x	x	x	x	x	100	a	0.5	0.2	500	70.44%
9/17/21	ML_Dataset_QA_NewPredicts	x	x	x	x	x	x	x	x	x	x	x	x	x	x	x	x	x	x	x	x	x	x	x	x	x	x	x	x	100	a	0.7	0.2	500	67.10%
9/17/21	ML_Dataset_QA_NewPredicts	x	x	x	x	x	x	x	x	x	x	x	x	x	x	x	x	x	x	x	x	x	x	x	x	x	x	x	x	150	a	0.5	0.2	500	70.44%
9/17/21	ML_Dataset_QA_NewPredicts	x	x	x	x	x	x	x	x	x	x	x	x	x	x	x	x	x	x	x	x	x	x	x	x	x	x	x	x	50	a	0.5	0.2	500	70.44%
9/17/21	ML_Dataset_QA_NewPredicts	x	x	x	x	x	x	x	x	x	x	x	x	x	x	x	x	x	x	x	x	x	x	x	x	x	x	x	x	100	a	0.5	0.4	500	67.61%
9/17/21	ML_Dataset_QA_NewPredicts	x	x	x	x	x	x	x	x	x	x	x	x	x	x	x	x	x	x	x	x	x	x	x	x	x	x	x	x	100	a	0.5	0.6	500	67.35%
9/17/21	ML_Dataset_QA_NewPredicts	x	x	x	x	x	x	x	x	x	x	x	x	x	x	x	x	x	x	x	x	x	x	x	x	x	x	x	x	100	a	0.5	0.5	500	68.12%
9/17/21	ML_Dataset_QA_NewPredicts	x	x	x	x	x	x	x	x	x	x	x	x	x	x	x	x	x	x	x	x	x	x	x	x	x	x	x	x	100	a	0.5	0.3	500	69.67%
9/17/21	ML_Dataset_QA_NewPredicts	x	x	x	x	x	x	x	x	x	x	x	x	x	x	x	x	x	x	x	x	x	x	x	x	x	x	x	x	100	a	0.5	0.2	1000	70.18%
9/17/21	ML_Dataset_QA_NewPredicts	x	x	x	x	x	x	x	x	x	x	x	x	x	x	x	x	x	x	x	x	x	x	x	x	x	x	x	x	100	a	0.5	0.2	250	70.95%
9/17/21	ML_Dataset_QA_NewPredicts	x	x	x	x	x	x	x	x	x	x	x	x	x	x	x	x	x	x	x	x	x	x	x	x	x	x	x	x	100	a	0.5	0.2	350	71.72%
9/17/21	ML_Dataset_QA_NewPredicts	x	x	x	x	x	x	x	x	x	x	x	x	x	x	x	x	x	x	x	x	x	x	x	x	x	x	x	x	100	a	0.5	0.2	400	70.44%
9/17/21	ML_Dataset_QA_NewPredicts	x	x	x	x	x	x	x	x	x	x	x	x	x	x	x	x	x	x	x	x	x	x	x	x	x	x	x	x	100	a	0.5	0.2	300	71.72%
9/17/21	ML_Dataset_QA_NewPredicts	x	x	x	x	x	x	x	x	x	x	x	x	x	x	x	x	x	x	x	x	x	x	x	x	x	x	x	x	100	a	0.5	0.2	325	71.47%
9/17/21	ML_Dataset_QA_NewPredicts	x	x	x	x	x	x	x	x	x	x	x	x	x	x	x	x	x	x	x	x	x	x	x	x	x	x	x	x	100	a	0.5	0.2	275	71.47%
9/17/21	ML_Dataset_QA_NewPredicts	x	x	x	x	x	x	x	x	x	x	x	x	x	x	x	x	x	x	x	x	x	x	x	x	x	x	x	x	100	0	0.5	0.2	300	70.69%
9/17/21	ML_Dataset_QA_NewPredicts	x	x	x	x	x	x	x	x	x	x	x	x	x	x	x	x	x	x	x	x	x	x	x	x	x	x	x	x	100	0	0.5	0.2	350	71.21%
9/17/21	ML_Dataset_QA_NewPredicts	x	x	x	x	x	x	x	x	x	x	x	x	x	x	x	x	x	x	x	x	x	x	x	x	x	x	x	x	100	0	0.5	0.2	400	71.98%
9/17/21	ML_Dataset_QA_NewPredicts	x	x	x	x	x	x	x	x	x	x	x	x	x	x	x	x	x	x	x	x	x	x	x	x	x	x	x	x	100	0	0.5	0.2	450	71.72%
9/17/21	ML_Dataset_QA_NewPredicts	x	x	x	x	x	x	x	x	x	x	x	x	x	x	x	x	x	x	x	x	x	x	x	x	x	x	x	x	100	i	0.5	0.2	300	70.18%
9/17/21	ML_Dataset_QA_NewPredicts	x	x	x	x	x	x	x	x	x	x	x	x	x	x	x	x	x	x	x	x	x	x	x	x	x	x	x	x	100	i	0.5	0.2	350	69.67%
9/17/21	ML_Dataset_QA_NewPredicts	x	x	x	x	x	x	x	x	x	x	x	x	x	x	x	x	x	x	x	x	x	x	x	x	x	x	x	x	100	i	0.5	0.2	400	70.44%
9/17/21	ML_Dataset_QA_NewPredicts	x	x	x	x	x	x	x	x	x	x	x	x	x	x	x	x	x	x	x	x	x	x	x	x	x	x	x	x	100	o	0.5	0.2	300	67.61%
9/17/21	ML_Dataset_QA_NewPredicts	x	x	x	x	x	x	x	x	x	x	x	x	x	x	x	x	x	x	x	x	x	x	x	x	x	x	x	x	100	o	0.5	0.2	350	66.32%
9/17/21	ML_Dataset_QA_NewPredicts	x	x	x	x	x	x	x	x	x	x	x	x	x	x	x	x	x	x	x	x	x	x	x	x	x	x	x	x	100	o	0.5	0.2	400	65.81%
9/17/21	ML_Dataset_QA_NewPredicts	x	x	x	x	x	x	x	x	x	x	x	x	x	x	x	x	x	x	x	x	x	x	x	x	x	x	x	x	100	t	0.5	0.2	300	68.89%
9/17/21	ML_Dataset_QA_NewPredicts	x	x	x	x	x	x	x	x	x	x	x	x	x	x	x	x	x	x	x	x	x	x	x	x	x	x	x	x	100	t	0.5	0.2	350	68.89%
9/17/21	ML_Dataset_QA_NewPredicts	x	x	x	x	x	x	x	x	x	x	x	x	x	x	x	x	x	x	x	x	x	x	x	x	x	x	x	x	100	t	0.5	0.2	400	69.92%
9/17/21	ML_Dataset_QA_NewPredicts	x	x	x	x	x	x	x	x	x	x	x	x	x	x	x	x	x	x	x	x	x	x	x	x	x	x	x	x	100	t	0.5	0.2	450	70.44%
9/17/21	ML_Dataset_QA_NewPredicts	x	x	x	x	x	x	x	x	x	x	x	x	x	x	x	x	x	x	x	x	x	x	x	x	x	x	x	x	100	t	0.5	0.2	500	70.18%
9/17/21	ML_Dataset_QA_NewPredicts	x	x	x	x	x	x	x	x	x	x	x	x	x	x	x	x	x	x	x	x	x	x	x	x	x	x	x	x	100	0	0.5	0.2	375	71.72%
9/28/21	ML_Dataset_QA_NewPredicts			x	x	x	x	x	x	x	x	x	x	x	x	x	x	x	x	x	x	x	x	x	x	x	x	x	x	100	0	0.5	0.2	400	70.18%
9/28/21	ML_Dataset_QA_NewPredicts	x	x			x	x	x	x	x	x	x	x	x	x	x	x	x	x	x	x	x	x	x	x	x	x	x	x	100	0	0.5	0.2	400	68.64%
9/28/21	ML_Dataset_QA_NewPredicts	x	x	x	x			x	x	x	x	x	x	x	x	x	x	x	x	x	x	x	x	x	x	x	x	x	x	100	0	0.5	0.2	400	69.15%
9/28/21	ML_Dataset_QA_NewPredicts	x	x	x	x	x	x			x	x	x	x	x	x	x	x	x	x	x	x	x	x	x	x	x	x	x	x	100	0	0.5	0.2	400	71.21%
9/28/21	ML_Dataset_QA_NewPredicts	x	x	x	x	x	x	x	x			x	x	x	x	x	x	x	x	x	x	x	x	x	x	x	x	x	x	100	0	0.5	0.2	400	72.75%
9/28/21	ML_Dataset_QA_NewPredicts	x	x	x	x	x	x	x	x	x	x			x	x	x	x	x	x	x	x	x	x	x	x	x	x	x	x	100	0	0.5	0.2	400	72.49%
9/28/21	ML_Dataset_QA_NewPredicts	x	x	x	x	x	x	x	x					x	x	x	x	x	x	x	x	x	x	x	x	x	x	x	x	100	0	0.5	0.2	400	73.01%
9/28/21	ML_Dataset_QA_NewPredicts	x	x	x	x	x	x	x	x	x	x	x	x	x	x	x	x	x	x						x	x	x	x	x	100	0	0.5	0.2	400	70.18%
9/28/21	ML_Dataset_QA_NewPredicts	x	x	x	x	x	x	x	x	x	x	x	x	x	x	x	x	x	x	x	x	x	x							100	0	0.5	0.2	400	69.92%
9/28/21	ML_Dataset_QA_NewPredicts	x	x	x	x	x	x	x	x	x	x	x	x							x	x	x	x	x	x	x	x	x	x	100	0	0.5	0.2	400	70.69%
9/28/21	ML_Dataset_QA_NewPredicts	x	x	x	x	x	x	x	x					x	x	x	x	x	x						x	x	x	x	x	100	0	0.5	0.2	400	69.67%
9/28/21	ML_Dataset_QA_NewPredicts	x	x	x	x	x	x	x	x					x	x	x	x	x	x	x	x	x	x	x						100	0	0.5	0.2	400	67.10%
9/28/21	ML_Dataset_QA_NewPredicts	x	x	x	x	x	x	x	x											x	x	x	x	x	x	x	x	x	x	100	0	0.5	0.2	400	70.69%
9/28/21	ML_Dataset_QA_NewPredicts	x	x	x	x	x	x	x	x					x		x	x			x		x	x		x		x	x		100	0	0.5	0.2	400	73.52%
9/28/21	ML_Dataset_QA_NewPredicts	x	x	x	x	x	x	x	x					x						x		x	x		x		x	x		100	0	0.5	0.2	400	74.04%
9/28/21	ML_Dataset_QA_NewPredicts	x	x	x	x	x	x	x	x					x						x					x		x	x		100	0	0.5	0.2	400	71.98%
9/28/21	ML_Dataset_QA_NewPredicts	x	x	x	x	x	x	x	x					x						x					x					100	0	0.5	0.2	400	69.92%
9/28/21	ML_Dataset_QA_NewPredicts	x	x	x		x		x						x						x					x					100	0	0.5	0.2	400	73.26%
9/28/21	ML_Dataset_QA_NewPredicts	x	x	x	x	x	x	x	x					x								x	x				x	x		100	0	0.5	0.2	400	73.52%
9/28/21	ML_Dataset_QA_NewPredicts	x	x	x	x	x	x	x	x					x						x		x	x		x		x	x		100	0	0.5	0.2	450	75.06%

APPENDIX B: R CODE

```
#Author: Jessica Richter
#Majority Vote Calculator for ML Ensemble Analysis
#Created: Oct. 27, 2021
#Last Updated: Oct. 29, 2021
#This script assesses the classification results of five machine learning algorithms and selects the classification based upon a majority vote and weighted vote (algorithm accuracy).
#Can be used for object-based or pixel-based analyses.

#Read .csv and .xls files
library(readr)
library(readxl)

#Load results from five individual algorithms
results <- read_csv("Pixel_TestingResults_Compiled_Expanded_pt1.csv")

#Create ensemble table where ensemble results will be populated
ensemble <- read_csv("Ensemble_results.csv")

#Initialize loop constants
i <- 1
j <- 1

#While loop is indexed at every 5 instances
while (i < 743192) {
        modified_sum <- 0
        bluff_sum <- 0
        marsh_sum <- 0
        swamp_sum <- 0
        low_sum <- 0
        high_sum <- 0

        #For loops through a window of 5 instances at a time; assigns accuracy % to each shoreclass value
        for (i in seq(from = i, to = i + 4)) {
                if (results$Result[i] == "1:modified_shoreline") {
                        modified_sum <- modified_sum + results$Accuracy[i]
                } else if (results$Result[i] == "2:natural_bluff") {
                        bluff_sum <- bluff_sum + results$Accuracy[i]
                } else if (results$Result[i] == "3:marsh") {
                        marsh_sum <- marsh_sum + results$Accuracy[i]
                } else if (results$Result[i] == "4:swamp_forest") {
                        swamp_sum <- swamp_sum + results$Accuracy[i]
                } else if (results$Result[i] == "5:low_sediment_bank") {
                        low_sum <- low_sum + results$Accuracy[i]
                } else if (results$Result[i] == "6:high_sediment_bank") {
                        high_sum <- high_sum + results$Accuracy[i]
                }
        }

        #Majority vote assigned to shoreline class with highest summed value, then result is populated in ensemble table
        sums <- c(modified_sum, bluff_sum, marsh_sum, swamp_sum, low_sum, high_sum)
        ensemble$ensemble_selection[j] <- which.max(sums)

        i <- i + 1
        j <- j + 1
}

#Export results
write.csv(ensemble, "pixel_ensembleresults_pt1.csv")
```

APPENDIX C: MACHINE LEARNING CLASSIFIER CONFUSION MATRICES

1. Confusion matrix for object-based ANN classifier.

Shoreline Classification	High Sediment Bank	Low Sediment Bank	Marsh	Modified Shoreline	Natural Bluff	Swamp Forest	Total	User's Accuracy (%)
High Sediment Bank	1	1	0	2	0	0	4	25.0%
Low Sediment Bank	2	55	1	12	0	2	72	76.4%
Marsh	0	5	51	1	2	2	61	83.6%
Modified Shoreline	7	14	2	135	17	3	178	75.8%
Natural Bluff	0	0	0	15	44	1	60	73.3%
Swamp Forest	2	1	1	3	1	6	14	42.9%
Total	12	76	55	168	64	14	Overall Accuracy:	
Producer's Accuracy (%)	8.3%	72.4%	92.7%	80.4%	68.8%	42.9%	75.1%	

2. Confusion matrix for object-based LibLINEAR classifier.

Shoreline Classification	High Sediment Bank	Low Sediment Bank	Marsh	Modified Shoreline	Natural Bluff	Swamp Forest	Total	User's Accuracy (%)
High Sediment Bank	4	1	0	0	1	0	6	66.7%
Low Sediment Bank	1	54	2	10	1	4	72	75.0%
Marsh	0	7	52	3	0	2	64	81.3%
Modified Shoreline	6	11	1	136	22	4	180	75.6%
Natural Bluff	0	2	0	19	39	0	60	65.0%
Swamp Forest	1	1	0	0	1	4	7	57.1%
Total	12	76	55	168	64	14	Overall Accuracy:	
Producer's Accuracy	33.3%	71.1%	94.5%	81.0%	60.9%	28.6%	74.3%	

3. Confusion matrix for object-based SVM classifier.

Shoreline Classification	High Sediment Bank	Low Sediment Bank	Marsh	Modified Shoreline	Natural Bluff	Swamp Forest	Total	User's Accuracy (%)
High Sediment Bank	3	1	0	1	0	0	5	60.0%
Low Sediment Bank	1	57	4	21	2	2	87	65.5%
Marsh	0	7	49	2	0	3	61	80.3%
Modified Shoreline	7	11	2	130	23	6	179	72.6%
Natural Bluff	0	0	0	12	39	0	51	76.5%
Swamp Forest	1	0	0	2	0	3	6	50.0%
Total	12	76	55	168	64	14	Overall Accuracy:	
Producer's Accuracy	25.0%	75.0%	89.1%	77.4%	60.9%	21.4%	72.2%	

4. Confusion matrix for object-based kNN classifier.

Shoreline Classification	High Sediment Bank	Low Sediment Bank	Marsh	Modified Shoreline	Natural Bluff	Swamp Forest	Total	User's Accuracy (%)
High Sediment Bank	0	0	0	1	0	0	1	0.0%
Low Sediment Bank	4	52	1	16	2	3	78	66.7%
Marsh	0	5	48	5	1	5	64	75.0%
Modified Shoreline	7	14	5	125	18	4	173	72.3%
Natural Bluff	1	4	0	21	43	1	70	61.4%
Swamp Forest	0	1	1	0	0	1	3	33.3%
Total	12	76	55	168	64	14	Overall Accuracy:	
Producer's Accuracy	0.0%	68.4%	87.3%	74.4%	67.2%	7.1%	69.2%	

5. Confusion matrix for object-based RF classifier.

Shoreline Classification	High Sediment Bank	Low Sediment Bank	Marsh	Modified Shoreline	Natural Bluff	Swamp Forest	Total	User's Accuracy (%)
High Sediment Bank	0	0	0	0	0	0	0	0.0%
Low Sediment Bank	0	57	1	11	0	1	70	81.4%
Marsh	0	6	54	3	0	7	70	77.1%
Modified Shoreline	11	13	0	139	25	6	194	71.6%
Natural Bluff	1	0	0	15	39	0	55	70.9%
Swamp Forest	0	0	0	0	0	0	0	0.0%
Total	12	76	55	168	64	14	Overall Accuracy:	
Producer's Accuracy	0.0%	75.0%	98.2%	82.7%	60.9%	0.0%	74.3%	